Recurrence of CAEBV with EBV-infected, donor-derived T cells following HSCT

The relative prevalence of CAEBV in East Asia and in natives of Central and South America implies a genetic background for its pathogenesis. Recently HLA-A*26, a major histocompatibility complex class I allele relatively common in East Asia, was found to be associated with an increased risk for EBV$^+$ T/NK-LPD.[35] Although the possible involvement of EBV strains with increased propensity to induce T/NK-cell lymphoproliferation cannot be formally denied, it is highly unlikely because outbreaks and familial transmission of CAEBV have not been reported. Arai *et al.* reported an intriguing case of CAEBV in which the patient experienced relapse after bone marrow transplantation.[36] A 35-year-old female patient with CAEBV of the CD8 type had HSCT from an unrelated male donor following myeloablative preconditioning with total body irradiation. The serologic HLA types of the patient and the donor were identical, whereas the DNA types were different in two HLA-DR alleles. Although the peripheral blood EBV-DNA was undetectable at 1 month after HSCT and remained so for nearly 12 months, the patient's EBV-DNA load increased again and reached 1.0×10^5 copies/μg DNA. EBV was found primarily in CD8$^+$ T cells again, but the EBV-infected cells now had an XY karyotype, clearly indicating their donor origin. Sequencing analysis of the variable region of the EBV-encoded *LMP1* gene showed that the virus strain infecting the CD8$^+$ T cells was different before and after bone marrow transplantation, suggesting that the repeated episodes of CAEBV were not caused by a rare EBV strain with an unusual biological activity. If we do not suppose that these two consecutive episodes of CAEBV in a single patient occurred only by chance, these findings suggest that the patient may have had a certain genetic background that exerts its direct effects on cellular lineages unrelated to hematopoietic stem cells.

Pathophysiology of CAEBV

The pathogenesis of CAEBV is not understood. Most T and NK cells do not express the EBV receptor CD21, and the mechanism of their infection with EBV is not clear. Transfer of CD21 from B cells to NK cells through immunological synapse may render the latter cells accessible to EBV.[37] The mechanism by which EBV induces proliferation of T and NK cells is not known either. EBV-induced expression of CD40 and its engagement by CD40L may have a role in the survival of EBV-infected T and NK cells of CAEBV patients.[38] Given that EBV-positive T or NK cells have been occasionally found in the tonsil and peripheral blood of IM patients, ectopic EBV infection in T or NK cells does not necessarily lead to the development of CAEBV.[39–41] Although EBV-infected T and NK cells in CAEBV patients and cell lines derived from them do not express the most immunodominant EBNA3 and EBNA2, they express EBNA1, latent membrane protein 1 (LMP1) and LMP2 (the latency II type EBV gene expression) that are frequently recognized by EBV-specific CTL.[3,42–45] Hosts with normal immune functions are thus expected to have the capacity to recognize EBV-infected T and NK cells. It is thus conceivable that patients with CAEBV have a certain defect in immunologic functions that causes inefficient recognition and/or killing of EBV-infected latency II cells. Indeed, deficiency in cellular immune responses to EBV has been detected in patients with CAEBV.[46–48]The defect in T-cell responses to LMP2A might be particularly relevant to this issue.[47] Interestingly, a patient with clinical manifestations similar to CAEBV, although the virus was found in his B cells, was found to have mutations in the gene encoding perforin, which has a critical role in granule-mediated killing of target cells.[49] None of the other patients with CAEBV, however, were found to have a mutation in the *perforin* gene. Mutations of the genes responsible for XLP, XIAP deficiency, and familial HLH (except for the type 2 that is caused by mutations of *perforin*) have not been reported for patients with CAEBV.[7]

Clonal proliferation of EBV-infected T or NK cells in CAEBV and other EBV$^+$ T/NK-LPD implies that these diseases have a malignant nature. CAEBV, however, is a chronic disease and patients with clonal expansion of EBV-infected T or NK cells may remain in a stable condition for years without treatment.[18] Overt malignant lymphoma occurs usually after a long course of disease. Therefore CAEBV may represent, at least in its early phase, a premalignant or smoldering phase of EBV-positive leukemia/lymphomas. Ohshima *et al.* proposed a pathological categorization of CAEBV into a continuous spectrum ranging from a smoldering phase to overt leukemia/lymphoma.[50] Clonality of EBV-infected T or NK cells in CAEBV may not necessarily indicate a malignant phenotype; acquisition of clonality might be a result of other selective processes such as immune escape.

Mouse xenograft models for EBV$^+$ T/NK-LPD

Animal models for EBV$^+$ T/NK-LPD have not been available, rendering research on their pathogenesis and therapy difficult. Imadome *et al.* transplanted peripheral blood mononuclear cells (PBMC) isolated from patients with CAEBV and EBV-HLH into immunodeficient mice of the NOD/Shi-*scid*/IL-2Rγ^{null} (NOG) strain, and successfully reproduced major features of these diseases including systemic monoclonal proliferation of EBV-infected T or NK cells and hypercytokinemia (Fig. 1).[51] Although many features were common to CAEBV and EBV-HLH model mice, hemorrhagic lesions in the abdominal and thoracic cavities and extreme hypercytokinemia were unique to the latter model, indicating that these mouse models reflect the differences in the pathophysiology of the original diseases. Importantly, these models revealed an essential role of CD4$^+$ T cells in the engraftment of EBV-infected T and NK cells. *In vivo* depletion of CD4$^+$ T cells following transplantation effectively prevented the engraftment of EBV-infected cells of not only the CD4$^+$ lineage but also the CD8$^+$ and CD56$^+$ lineages. Furthermore, OKT-4 antibody given after engraftment was also effective to reduce EBV-DNA load in the peripheral blood and major organs (Imadome *et al.*, unpubl. data 2012). These results suggest that therapeutic approaches targeting CD4$^+$ T cells may be possible.

Diagnosis and monitoring of CAEBV

Prolonged or relapsing symptoms of IM are the major clue to the diagnosis of CAEBV. Although elevated serum antibody titers

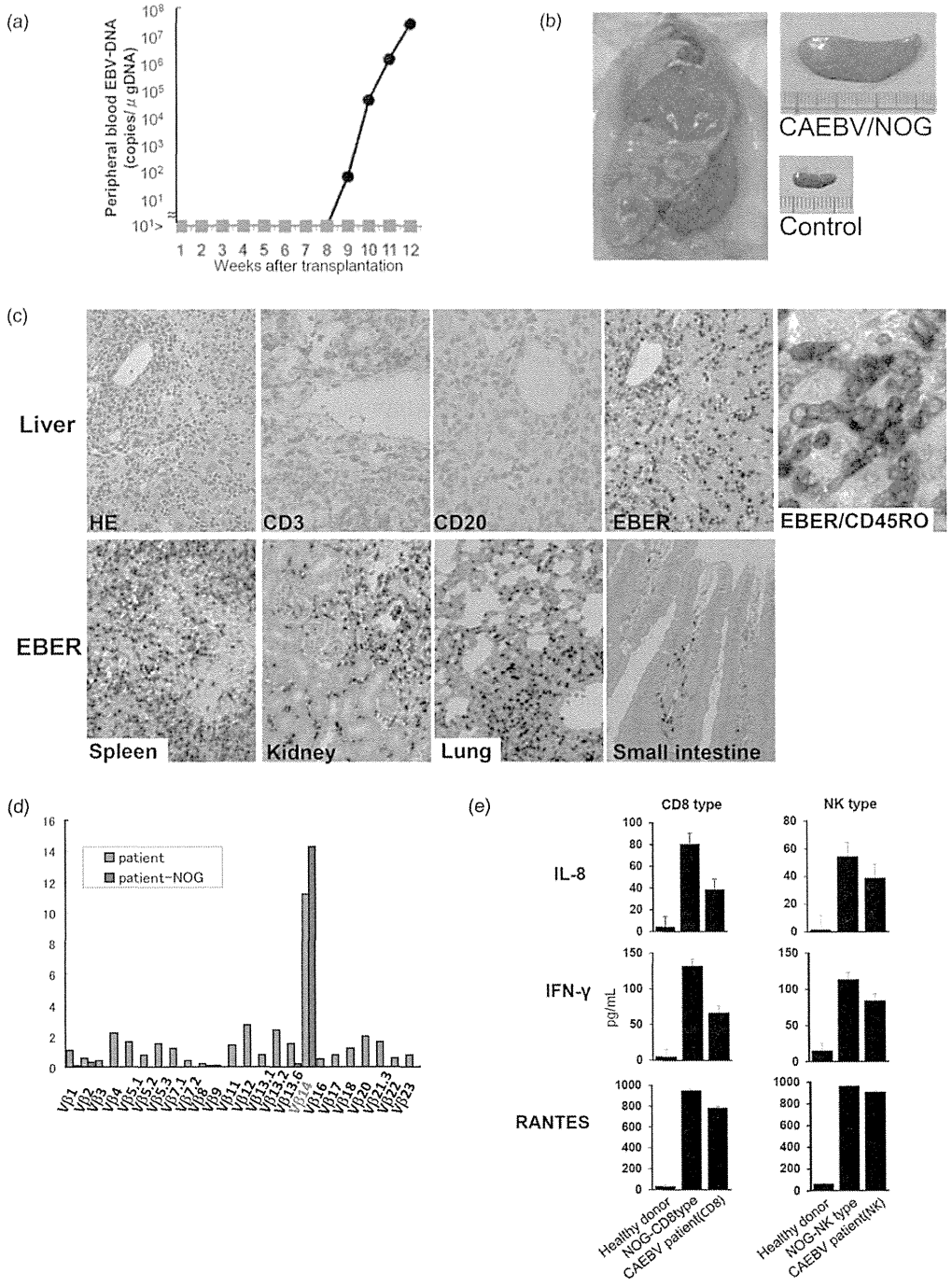

Fig. 1 Mouse xenograft model of chronic active Epstein–Barr virus infection (CAEBV). Peripheral blood mononuclear cells (PBMC) of a patient with the CD8 type CAEBV were transplanted i.v. into NOD/Shi-*scid Il2rg* ^{null} (NOG) mice. (a) Measurement of peripheral blood EBV-DNA. EBV-DNA load increased rapidly from approximately 9 weeks after transplantation, when (●) whole PBMC but not (□) isolated $CD8^+$ cells were transplanted. (b) Splenomegaly of a model mouse. (c) Pathological analysis. Histochemical analysis showed massive infiltration of EBV-encoded small RNA $(EBER)^+/CD20^-/CD3^+/CD45RO^+$ cells in most major organs including the spleen, kidneys, lungs, and small intestine. (d) T-cell receptor (TCR) repertoire analysis of peripheral blood T cells isolated from the patient and a mouse that received the patient's PBMC. An identical clone of EBV-infected T cells expressing Vβ14 is proliferating in the patient and the corresponding mouse. (e) Human cytokine levels in CAEBV model mice. Serum levels of interleukin (IL)-8, interferon (IFN)-γ, and regulated on activation, normal T-cell expressed and secreted (RANTES) were measured in mice that were transplanted with PBMC isolated from either a CD8-type or an NK-type CAEBV patient. The same set of cytokines was also quantified in the sera of the original patients and healthy donors. Modified from *PLoS Pathog.* 2011; **7**(10): e1002326.[51]

against EBV-encoded antigens are often found, this does not always occur, and normal titers of anti-EBV antibodies should not preclude the diagnosis of CAEBV.[7] Diagnostic criteria for CAEBV have been published.[13] Quantification of peripheral blood EBV-DNA is most important for diagnosis and a finding of elevation should be followed by identification of EBV-infected T or NK cells. Quantification of EBV-DNA is, however, influenced by many factors and the results can vary in different laboratories.[52] Recently, therefore, an international standard EBV-DNA sample for normalization became available from the National Institute for Biological Standards and Controls, USA. Given that CAEBV is a chronic disease that may progress to overt malignancy and early HSCT in a better clinical condition is recommended, precise monitoring of patient clinical parameters is particularly important.

Flow-cytometric in situ *hybridization for identification of EBV-infected cells*

Diagnosis of CAEBV requires exact phenotyping of EBV-infected cells. This has usually been done with immunobead sorting of PBMC into lymphocyte subsets, followed by measurement of EBV-DNA in each subset using quantitative polymerase chain reaction. These processes are, however, time-consuming and require specific skills. Kimura *et al.* developed a new method termed "flow-cytometric *in situ* hybridization" (FISH) to phenotype EBV-infected cells (Fig. 2).[53,54] They utilized a fluorescence-labeled peptide nucleic acid (PNA) probe complementary to EBER and succeeded in detecting EBER on flow cytometry. Following reaction with antibodies specific to surface markers, PBMC were permeabilized and subjected to *in situ* hybridization with the PNA probe. EBER probes and surface-bound antibodies were then detected simultaneously on flow cytometry. EBV-infected cells with a certain phenotype can be directly counted using FISH, which is less laborious than the current method. They showed that FISH can be applied for the diagnosis of EBV$^+$ T/NK-LPD, and that EBV infects mainly γδT cells in HV.[53–55]

MicroRNA as a potential biomarker of CAEBV

MicroRNA (miRNA) is a small non-coding RNA of 18–25 nucleotides that plays a critical role in the regulation of cellular proliferation, differentiation, and apoptosis through negatively regulating mRNA translation.[56] miRNAs are encoded not only by cells but also by viruses; EBV is actually the first virus shown to encode miRNAs.[57] Two clusters of EBV-encoded miRNAs have been identified: miR–*Bam*HI fragment H rightward open reading frame 1 (miR-BHRF1) and miR–*Bam* HI A region rightward transcripts (miR-BART).[58] Kawano *et al.* reported that plasma levels of miR-BART 1-5p, 2-5p, 5, and 22 are significantly higher in patients with CAEBV than in those with IM and healthy controls.[59] Plasma miR-BART 2-5p, 4, 7, 13, 15, and 22 levels were significantly elevated in CAEBV patients with active disease compared to those with inactive disease. miR-BART 13 level could differentiate patients with active disease from those with inactive disease, with a clear cut-off. Similarly, plasma miR-BART 2-5p and 15 levels could clearly differentiate patients with complete remission from others. Importantly, plasma EBV-DNA level did not show any significant correlation with these clinical parameters. These results suggest that EBV-encoded miRNA in plasma may be a useful biomarker for the diagnosis and monitoring of CAEBV.

Therapy of CAEBV

Various therapies have been tried for the treatment of CAEBV, including antiviral, chemotherapeutic, and immunomodulatory drugs, with only limited success. These regimens induced sustained complete remission in only exceptional cases and HSCT is at present the only curative therapy for CAEBV.[60] The current event-free survival rate for CAEBV patients following HSCT is estimated to be 0.561 ± 0.086.[61]Very recently, Kawa *et al.* reported excellent results of HSCT following non-destructive pretreatment (reduced intensity hematopoietic stem cell transplantation; RIST).[62] For 18 pediatric patients with CAEBV who were treated with RIST, 3 year event-free survival was $85.0 \pm 8.0\%$ and the 3 year overall survival rate was $95.0 \pm 4.9\%$. HSCT is thus the therapy of choice for CAEBV, but HSCT is still accompanied by substantial risk and CAEBV patients have high risk for transplantation-related complications.[18] It is therefore desirable to develop novel therapies that do not depend on HSCT. Preclinical studies of two candidate drugs for CAEBV have been carried out recently and gave hopeful results.

Bortezomib, known as an inhibitor of 26S proteasome,[63] also has an inhibitory effect on the cellular transcription factor NF-κB. Because the survival and proliferation of EBV-transformed B cells are critically dependent on NF-κB activity, bortezomib has been shown to induce apoptosis in these cells.[64] Iwata *et al.* investigated the effect of bortezomib on EBV-infected T-cell lines including those derived from CAEBV.[65] Bortezomib induced apoptosis in all human T-cell lymphoma cell lines examined, whether or not they were infected with EBV. In addition, bortezomib induced the expression of EBV lytic-cycle genes *BZLF1* and *gp350/220*, as has been reported for EBV-infected B-cell lines.[66] Bortezomib also induced apoptosis specifically in EBV-infected T or NK cells cultured *ex vivo* from patients with EBV$^+$T/NK-LPD.

Valproic acid is a widely used anti-epileptic drug and is also known as a potent histone deacetylase (HDAC) inhibitor. HDAC inhibitors have potent anticancer activities with proven efficacy in various human malignancies. Valproic acid induces lytic infection in EBV-infected B-lymphoblastoid and gastric carcinoma cell lines and thereby potentiates the effects of chemotherapeutic agents both *in vitro* and *in vivo*.[67] Iwata *et al.* examined the effect of valproic acid on EBV-infected T and NK cell lines.[68] They found that this agent induces apoptosis in human EBV-infected T and NK cells. Use of the drug with the NF-κB inhibitor bortezomib had an additive effect. In contrast to the previous results with EBV-infected B-cell lines, valproic acid did not induce lytic infection in the virus-infected T- and NK-cell lines, indicating that the apoptosis-inducing effect of valproic acid is not dependent on induction of EBV lytic cycle.

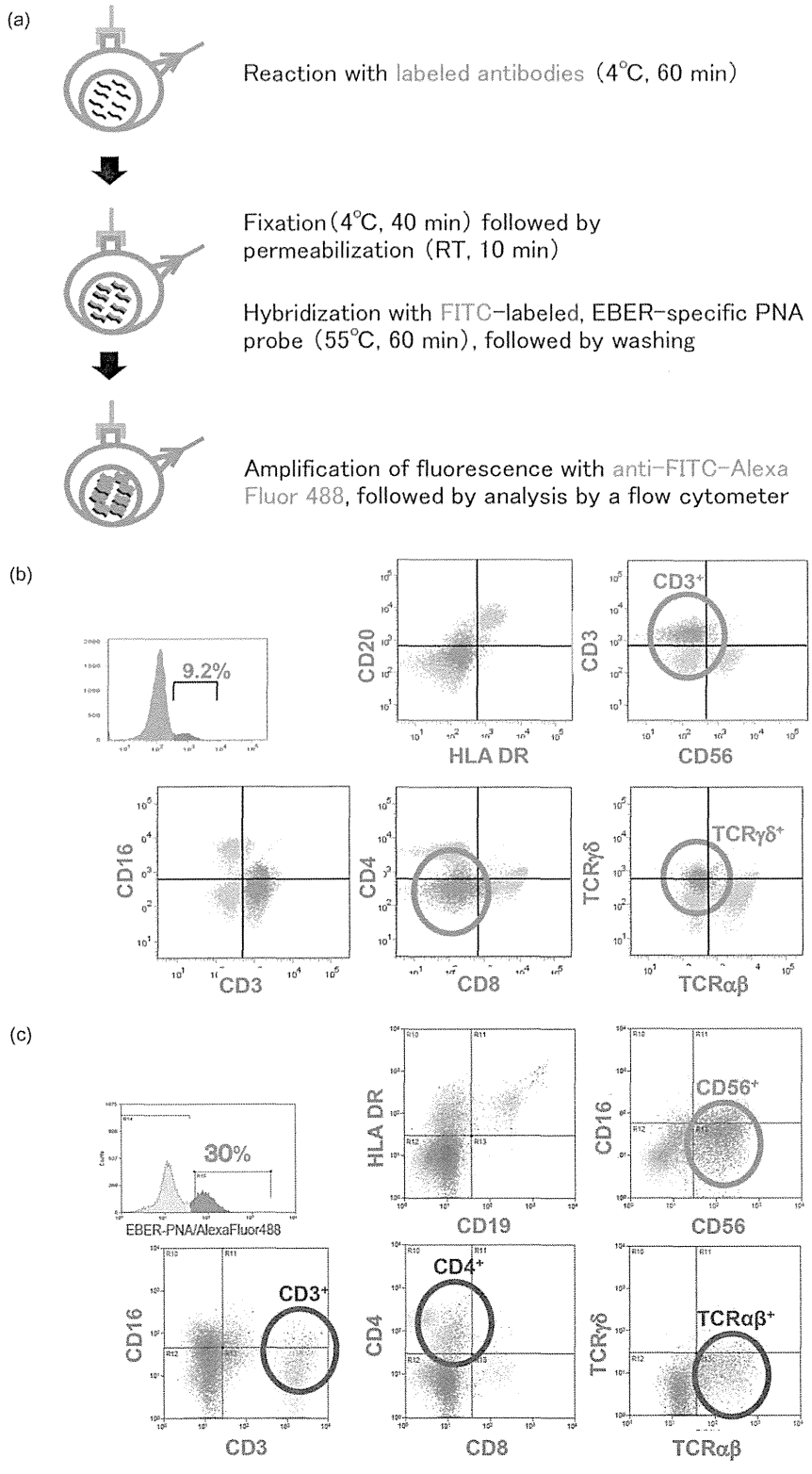

Fig. 2 Flow-cytometric *in situ* hybridization (FISH). (a) Protocol of FISH. (b) Results of FISH in a patient with hydroa vacciniforme. Red, EBER-positive cells; blue, EBER-negative cells. Most EBV-infected cells in the peripheral blood of this patient had the phenotype $CD3^+/CD4^-/CD8^-/TCR\gamma\delta^+$. (c) Results of FISH in a patient with the NK-cell type chronic active Epstein–Barr virus infection. Red, EBER-positive cells; blue, EBER-negative cells. The majority of EBV-infected cells in the peripheral blood of this patient were $CD56^+$ NK cells. Also, a small proportion of $TCR\alpha\beta^+/CD3^+/CD4^+$ cells also contained EBV. EBER, Epstein–Barr virus-encoded small RNA; FITC, fluorescein isothiocyanate; PNA, peptide nucleic acid; RT, reverse transcription.

Perspective

Significant progress has been made in the research of many aspects of CAEBV, including pathophysiology, diagnosis, monitoring, and therapy, but the fundamental cause of the disease has not been elucidated. The recent development of novel technologies for genetic analysis, including new-generation sequencing, may enable identification of genetic alterations responsible for CAEBV. Given that CAEBV is an uncommon disease, it may sometimes take years for the correct diagnosis to be reached. The advanced techniques required for this also make the diagnosis of CAEBV difficult. Although there is a consensus that early HSCT produces a better result, the decision to have HSCT is often difficult, especially when the patient is in a stable condition without severe symptoms. Establishing a standard clinical guideline for the diagnosis and treatment of CAEBV will alleviate these problems and facilitate quick and accurate diagnosis, followed by timely intervention with the right choice of treatment.

Acknowledgments

The authors' works described in this article have been funded by grants from the Ministry of Health Labour and Welfare of Japan for the Research on Measures for Intractable Diseases (H21-Nanchi-094, H22-Nanchi-080, H24-Nanchi-046).

References

1 Epstein MA, Achong BG, Barr YM. Virus particles in cultured lymphoblasts from Burkitt's lymphoma. *Lancet* 1964; **1**: 702–3.
2 Longnecker RM, Kieff E, Cohen JI. Epstein-Barr virus. In: Knipe DM, Howley PM (eds). *Fields Virology*, Vol. **2**, 6th edn. Lippincott Williams and Wilkins, Philadelphia, PA, 2013; 1898–959.
3 Hislop AD, Taylor GS, Sauce D, Rickinson AB. Cellular responses to viral infection in humans: Lessons from Epstein-Barr virus. *Annu. Rev. Immunol.* 2007; **25**: 587–617.
4 Rickinson AB. Chronic, symptomatic Epstein-Barr virus infection. *Immunol. Today* 1986; **7**: 13–14.
5 Straus SE. The chronic mononucleosis syndrome. *J. Infect. Dis.* 1988; **157**: 405–12.
6 Okano M. Overview and problematic standpoints of severe chronic active Epstein-Barr virus infection syndrome. *Crit. Rev. Oncol. Hematol.* 2002; **44**: 273–82.
7 Kimura H. Pathogenesis of chronic active Epstein-Barr virus infection: Is this an infectious disease, lymphoproliferative disorder, or immunodeficiency? *Rev. Med. Virol.* 2006; **16**: 251–61.
8 Kikuta H, Taguchi Y, Tomizawa K *et al.* Epstein-Barr virus genome-positive T lymphocytes in a boy with chronic active EBV infection associated with Kawasaki-like disease. *Nature* 1988; **333**: 455–7.
9 Jones JF, Shurin S, Abramowsky C *et al.* T-cell lymphomas containing Epstein-Barr viral DNA in patients with chronic Epstein-Barr virus infections. *N. Engl. J. Med.* 1988; **318**: 733–41.
10 Ishihara S, Tawa A, Yumura-Yagi K *et al.* Clonal T-cell lymphoproliferation containing Epstein-Barr (EB) virus DNA in a patient with chronic active EB virus infection. *Jpn J. Cancer Res.* 1989; **80**: 99–101.
11 Kawa-Ha K, Ishihara S, Ninomiya T *et al.* CD3-negative lymphoproliferative disease of granular lymphocytes containing Epstein-Barr viral DNA. *J. Clin. Invest.* 1989; **84**: 51–5.
12 Cohen JI, Jaffe ES, Dale JK *et al.* Characterization and treatment of chronic active Epstein-Barr virus disease: A 28-year experience in the United States. *Blood* 2011; **117**: 5835–49.
13 Okano M, Kawa K, Kimura H *et al.* Proposed guidelines for diagnosing chronic active Epstein-Barr virus infection. *Am. J. Hematol.* 2005; **80**: 64–9.
14 Lay JD, Tsao CJ, Chen JY, Kadin ME, Su IJ. Upregulation of tumor necrosis factor-alpha gene by Epstein-Barr virus and activation of macrophages in Epstein-Barr virus-infected T cells in the pathogenesis of hemophagocytic syndrome. *J. Clin. Invest.* 1997; **100**: 1969–79.
15 Xu J, Ahmad A, Jones JF *et al.* Elevated serum transforming growth factor beta1 levels in Epstein-Barr virus-associated diseases and their correlation with virus-specific immunoglobulin A (IgA) and IgM. *J. Virol.* 2000; **74**: 2443–6.
16 Ohga S, Nomura A, Takada H *et al.* Epstein-Barr virus (EBV) load and cytokine gene expression in activated T cells of chronic active EBV infection. *J. Infect. Dis.* 2001; **183**: 1–7.
17 Kimura H, Hoshino Y, Kanegane H *et al.* Clinical and virologic characteristics of chronic active Epstein-Barr virus infection. *Blood* 2001; **98**: 280–86.
18 Kimura H, Morishima T, Kanegane H *et al.* Prognostic factors for chronic active Epstein-Barr virus infection. *J. Infect. Dis.* 2003; **187**: 527–33.
19 Jaffe ES. The 2008 WHO classification of lymphomas: Implications for clinical practice and translational research. *Hematology Am. Soc. Hematol. Educ. Program* 2009; 523–31.
20 Henter JI, Horne A, Arico M *et al.* HLH-2004: Diagnostic and therapeutic guidelines for hemophagocytic lymphohistiocytosis. *Pediatr. Blood Cancer* 2007; **48**: 124–31.
21 Kikuta H, Sakiyama Y, Matsumoto S *et al.* Fatal Epstein-Barr virus-associated hemophagocytic syndrome. *Blood* 1993; **82**: 3259–64.
22 Kawaguchi H, Miyashita T, Herbst H *et al.* Epstein-Barr virus-infected T lymphocytes in Epstein-Barr virus-associated hemophagocytic syndrome. *J. Clin. Invest.* 1993; **92**: 1444–50.
23 Yang X, Miyawaki T, Kanegane H. SAP and XIAP deficiency in hemophagocytic lymphohistiocytosis. *Pediatr. Int.* 2012; **54**: 447–54.
24 Goldgeier MH, Nordlund JJ, Lucky AW, Sibrack LA, McCarthy MJ, McGuire J. Hydroa vacciniforme: Diagnosis and therapy. *Arch. Dermatol.* 1982; **118**: 588–91.
25 Iwatsuki K, Xu Z, Takata M *et al.* The association of latent Epstein-Barr virus infection with hydroa vacciniforme. *Br. J. Dermatol.* 1999; **140**: 715–21.
26 Iwatsuki K, Ohtsuka M, Akiba H, Kaneko F. Atypical hydroa vacciniforme in childhood: From a smoldering stage to Epstein-Barr virus-associated lymphoid malignancy. *J. Am. Acad. Dermatol.* 1999; **40**: 283–4.
27 Ishihara S, Ohshima K, Tokura Y *et al.* Hypersensitivity to mosquito bites conceals clonal lymphoproliferation of Epstein-Barr viral DNA-positive natural killer cells. *Jpn J. Cancer Res.* 1997; **88**: 82–7.
28 Kawa K, Okamura T, Yagi K, Takeuchi M, Nakayama M, Inoue M. Mosquito allergy and Epstein-Barr virus-associated T/natural killer-cell lymphoproliferative disease. *Blood* 2001; **98**: 3173–4.
29 Ishihara S, Okada S, Wakiguchi H, Kurashige T, Hirai K, Kawa-Ha K. Clonal lymphoproliferation following chronic active Epstein-Barr virus infection and hypersensitivity to mosquito bites. *Am. J. Hematol.* 1997; **54**: 276–81.
30 Iwatsuki K, Yamamoto T, Tsuji K *et al.* A spectrum of clinical manifestations caused by host immune responses against Epstein-Barr virus infections. *Acta Med. Okayama* 2004; **58**: 169–80.
31 Kimura H, Ito Y, Kawabe S *et al.* EBV-associated T/NK-cell lymphoproliferative diseases in nonimmunocompromised hosts: Prospective analysis of 108 cases. *Blood* 2012; **119**: 673–86.
32 Isobe Y, Aritaka N, Setoguchi Y *et al.* T/NK cell type chronic active Epstein-Barr virus disease in adults: An underlying condition for Epstein-Barr virus-associated T/NK-cell lymphoma. *J. Clin. Pathol.* 2012; **65**: 278–82.

33 Takahashi E, Ohshima K, Kimura H *et al.* Clinicopathological analysis of the age-related differences in patients with Epstein-Barr virus (EBV)-associated extranasal natural killer (NK)/T-cell lymphoma with reference to the relationship with aggressive NK cell leukaemia and chronic active EBV infection-associated lymphoproliferative disorders. *Histopathology* 2011; **59**: 660–71.
34 Arai A, Imadome K, Watanabe Y *et al.* Clinical features of adult-onset chronic active Epstein-Barr virus infection: A retrospective analysis. *Int. J. Hematol.* 2011; **93**: 602–9.
35 Ito Y Sr, Torii Y, Kawa K, Kikuta A, Kojima S, Kimura H. HLA-A*26 and HLA-B*52 are associated with a risk of developing EBV-associated T/NK lymphoproliferative disease. *Blood* 2013; ID: bloodjournal_el; 8085.
36 Arai A, Imadome K, Wang L *et al.* Recurrence of chronic active Epstein-Barr virus infection from donor cells after achieving complete response through allogeneic bone marrow transplantation. *Intern. Med.* 2012; **51**: 777–82.
37 Tabiasco J, Vercellone A, Meggetto F, Hudrisier D, Brousset P, Fournie JJ. Acquisition of viral receptor by NK cells through immunological synapse. *J. Immunol.* 2003; **170**: 5993–8.
38 Imadome K, Shimizu N, Arai A *et al.* Coexpression of CD40 and CD40 ligand in Epstein-Barr virus-infected T and NK cells and their role in cell survival. *J. Infect. Dis.* 2005; **192**: 1340–48.
39 Anagnostopoulos I, Hummel M, Kreschel C, Stein H. Morphology, immunophenotype, and distribution of latently and/or productively Epstein-Barr virus-infected cells in acute infectious mononucleosis: Implications for the interindividual infection route of Epstein-Barr virus. *Blood* 1995; **85**: 744–50.
40 Hudnall SD, Ge Y, Wei L, Yang NP, Wang HQ, Chen T. Distribution and phenotype of Epstein-Barr virus-infected cells in human pharyngeal tonsils. *Mod. Pathol.* 2005; **18**: 519–27.
41 Kasahara Y, Yachie A, Takei K *et al.* Differential cellular targets of Epstein-Barr virus (EBV) infection between acute EBV-associated hemophagocytic lymphohistiocytosis and chronic active EBV infection. *Blood* 2001; **98**: 1882–8.
42 Imai S, Sugiura M, Oikawa O *et al.* Epstein-Barr virus (EBV)-carrying and -expressing T-cell lines established from severe chronic active EBV infection. *Blood* 1996; **87**: 1446–57.
43 Yoshioka M, Ishiguro N, Ishiko H, Ma X, Kikuta H, Kobayashi K. Heterogeneous, restricted patterns of Epstein-Barr virus (EBV) latent gene expression in patients with chronic active EBV infection. *J. Gen. Virol.* 2001; **82**: 2385–92.
44 Kimura H, Hoshino Y, Hara S *et al.* Differences between T cell-type and natural killer cell-type chronic active Epstein-Barr virus infection. *J. Infect. Dis.* 2005; **191**: 531–9.
45 Demachi A, Nagata H, Morio T *et al.* Characterization of Epstein-Barr virus (EBV)-positive NK cells isolated from hydroa vacciniforme-like eruptions. *Microbiol. Immunol.* 2003; **47**: 543–52.
46 Tsuge I, Morishima T, Kimura H, Kuzushima K, Matsuoka H. Impaired cytotoxic T lymphocyte response to Epstein-Barr virus-infected NK cells in patients with severe chronic active EBV infection. *J. Med. Virol.* 2001; **64**: 141–8.
47 Sugaya N, Kimura H, Hara S *et al.* Quantitative analysis of Epstein-Barr virus (EBV)-specific CD8+ T cells in patients with chronic active EBV infection. *J. Infect. Dis.* 2004; **190**: 985–8.
48 Fujieda M, Wakiguchi H, Hisakawa H, Kubota H, Kurashige T. Defective activity of Epstein-Barr virus (EBV) specific cytotoxic T lymphocytes in children with chronic active EBV infection and in their parents. *Acta Paediatr. Jpn* 1993; **35**: 394–9.
49 Katano H, Ali MA, Patera AC *et al.* Chronic active Epstein-Barr virus infection associated with mutations in perforin that impair its maturation. *Blood* 2004; **103**: 1244–52.
50 Ohshima K, Kimura H, Yoshino T *et al.* Proposed categorization of pathological states of EBV-associated T/natural killer-cell lymphoproliferative disorder (LPD) in children and young adults: Overlap with chronic active EBV infection and infantile fulminant EBV T-LPD. *Pathol. Int.* 2008; **58**: 209–17.
51 Imadome K, Yajima M, Arai A *et al.* Novel mouse xenograft models reveal a critical role of CD4+ T cells in the proliferation of EBV-infected T and NK cells. *PLoS Pathog.* 2011; **7**: e1002326.
52 Ito Y, Takakura S, Ichiyama S *et al.* Multicenter evaluation of prototype real-time PCR assays for Epstein-Barr virus and cytomegalovirus DNA in whole blood samples from transplant recipients. *Microbiol. Immunol.* 2010; **54**: 516–22.
53 Kimura H, Miyake K, Yamauchi Y *et al.* Identification of Epstein-Barr virus (EBV)-infected lymphocyte subtypes by flow cytometric in situ hybridization in EBV-associated lymphoproliferative diseases. *J. Infect. Dis.* 2009; **200**: 1078–87.
54 Kawabe S, Ito Y, Gotoh K *et al.* Application of flow cytometric in situ hybridization assay to Epstein-Barr virus-associated T/natural killer cell lymphoproliferative diseases. *Cancer Sci.* 2012; **103**: 1481–8.
55 Hirai Y, Yamamoto T, Kimura H *et al.* Hydroa vacciniforme is associated with increased numbers of Epstein-Barr virus-infected gammadeltaT cells. *J. Invest. Dermatol.* 2012; **132**: 1401–8.
56 Bartel DP. MicroRNAs: Target recognition and regulatory functions. *Cell* 2009; **136**: 215–33.
57 Pfeffer S, Zavolan M, Grasser FA *et al.* Identification of virus-encoded microRNAs. *Science* 2004; **304**: 734–6.
58 Cai X, Schafer A, Lu S *et al.* Epstein-Barr virus microRNAs are evolutionarily conserved and differentially expressed. *PLoS Pathog.* 2006; **2**: e23.
59 Kawano Y, Iwata S, Kawada J *et al.* Plasma viral microRNA profiles reveal potential biomarkers for chronic active Epstein-Barr virus infection. *J. Infect. Dis.* 2013; **208**: 771–9.
60 Okamura T, Hatsukawa Y, Arai H, Inoue M, Kawa K. Blood stem-cell transplantation for chronic active Epstein-Barr virus with lymphoproliferation. *Lancet* 2000; **356**: 223–4.
61 Sato E, Ohga S, Kuroda H *et al.* Allogeneic hematopoietic stem cell transplantation for Epstein-Barr virus-associated T/natural killer-cell lymphoproliferative disease in Japan. *Am. J. Hematol.* 2008; **83**: 721–7.
62 Kawa K, Sawada A, Sato M *et al.* Excellent outcome of allogeneic hematopoietic SCT with reduced-intensity conditioning for the treatment of chronic active EBV infection. *Bone Marrow Transplant.* 2011; **46**: 77–83.
63 Adams J. Proteasome inhibition: A novel approach to cancer therapy. *Trends Mol. Med.* 2002; **8**: S49–54.
64 Zou P, Kawada J, Pesnicak L, Cohen JI. Bortezomib induces apoptosis of Epstein-Barr virus (EBV)-transformed B cells and prolongs survival of mice inoculated with EBV-transformed B cells. *J. Virol.* 2007; **81**: 10029–36.
65 Iwata S, Yano S, Ito Y *et al.* Bortezomib induces apoptosis in T lymphoma cells and natural killer lymphoma cells independent of Epstein-Barr virus infection. *Int. J. Cancer* 2011; **129**: 2263–73.
66 Fu DX, Tanhehco YC, Chen J *et al.* Virus-associated tumor imaging by induction of viral gene expression. *Clin. Cancer Res.* 2007; **13**: 1453–8.
67 Feng WH, Kenney SC. Valproic acid enhances the efficacy of chemotherapy in EBV-positive tumors by increasing lytic viral gene expression. *Cancer Res.* 2006; **66**: 8762–9.
68 Iwata S, Saito T, Ito Y *et al.* Antitumor activities of valproic acid on Epstein-Barr virus-associated T and natural killer lymphoma cells. *Cancer Sci.* 2012; **103**: 375–81.

Molecular and Virological Evidence of Viral Activation From Chromosomally Integrated Human Herpesvirus 6A in a Patient With X-Linked Severe Combined Immunodeficiency

Akifumi Endo,[1,2] Ken Watanabe,[3] Tamae Ohye,[4] Kyoko Suzuki,[5] Tomoyo Matsubara,[5] Norio Shimizu,[3] Hiroki Kurahashi,[4] Tetsushi Yoshikawa,[6] Harutaka Katano,[7] Naoki Inoue,[8] Kohsuke Imai,[1] Masatoshi Takagi,[1] Tomohiro Morio,[1] and Shuki Mizutani[1]

[1]Department of Pediatrics and Developmental Biology, Tokyo Medical and Dental University, [2]Department of Pediatrics, Tokyo Metropolitan Cancer and Infectious Diseases Center, Komagome Hospital, and [3]Department of Virology, Tokyo Medical and Dental University, [4]Division of Molecular Genetics, Fujita Health University, Toyoake; [5]Department of Pediatrics, Juntendo University Urayasu Hospital, [6]Department of Pediatrics, Fujita Health University, Toyoake, Departments of [7]Pathology and [8]Virology I, National Institute of Infectious Diseases, Tokyo, Japan

(See the Editorial Commentary by Flamand on pages 549–51.)

It has been unclear whether chromosomally integrated human herpesvirus 6 (ciHHV-6) can be activated with pathogenic effects on the human body. We present molecular and virological evidence of ciHHV-6A activation in a patient with X-linked severe combined immunodeficiency. These findings have significant implications for the management of patients with ciHHV-6.

Keywords. ciHHV-6; HHV-6; X-SCID; hemophagocytic syndrome; thrombotic microangiopathy.

Human herpesvirus 6 (HHV-6) is a ubiquitous DNA virus that is the causative agent of roseola infantum, and infects individuals by 3 years of age [1]. After primary infection, HHV-6 establishes a latent state in the host. There are 2 distinct species, HHV-6A and HHV-6B. Most HHV-6 infections are caused by HHV-6B, whereas HHV-6A is less common. Chromosomally integrated HHV-6 (ciHHV-6) is the state in which HHV-6 (HHV-6A or HHV-6B) is integrated into the host germline genome, and it is transmitted vertically in a Mendelian manner. Although ciHHV-6 affects about 1% of the general population, it is generally considered to be a nonpathogenic condition. However, it is unclear whether ciHHV-6 can be activated with pathogenic effects on the human body [2].

Severe combined immunodeficiency (SCID) is a group of genetic disorders that result in a combined absence of T- and B-cell immunity. It is characterized by life-threatening infections during the first year of life unless treated, usually with hematopoietic stem cell transplantation (HSCT). X-linked severe combined immunodeficiency (X-SCID) arises from a mutation in the interleukin 2 receptor, gamma (*IL2RG*) gene on the X-chromosome [3]. We encountered a boy with X-SCID in whom ciHHV-6A was activated.

CASE REPORT

A 2-month-old boy was hospitalized for recurrent episodes of fever, cough, diarrhea, and failure to thrive. Upon admission, a viral infection was suspected, and supportive care did not improve his symptoms.

Twenty days after admission, mild pancytopenia (leukocyte count, 1.4×10^9/L; hemoglobin level, 78 g/L; and platelet count, 37×10^9/L) and elevated aminotransferases and ferritin were evident (aspartate aminotransferase, 448 U/L; alanine aminotransferase, 218 U/L; and ferritin, 4325 ng/mL) (Supplementary Figure 1). A bone marrow biopsy showed a hypocellular condition without dysplastic changes, as well as increased activated phagocytes. These results suggested hemophagocytic syndrome (HPS).

An immunological evaluation revealed an absence of T cells and low immunoglobulin levels. Genetic analysis identified a mutation in the *IL2RG* that was consistent with X-SCID. The patient's mother was heterozygous for the same mutation, and there was no such mutation detected in the patient's father.

A comprehensive search for a pathogen identified high levels of HHV-6 DNA (1.2×10^7 copies/μg DNA) in his peripheral blood. Antiviral treatment with ganciclovir or foscarnet did not reduce the viral load, and ciHHV-6 was suspected. We detected high levels of HHV-6 DNA in the patient's fingernails, the father's peripheral blood, and the father's hair follicles (5.9×10^5, 1.0×10^7, 1.2×10^6 copies/μgDNA, respectively).

Received 7 January 2014; accepted 9 April 2014; electronically published 6 May 2014.

Correspondence: Shuki Mizutani, MD, Department of Pediatrics and Developmental Biology, Tokyo Medical and Dental University, 1-5-45, Yushima, Bunkyo-ku, Tokyo 113-8510, Japan (skkmiz@gmail.com).

Clinical Infectious Diseases 2014;59(4):545–8

DOI: 10.1093/cid/ciu323

Fluorescence in situ hybridization analysis of the patient's fibroblasts and his father's peripheral blood mononuclear cells (PBMCs) confirmed HHV-6 integration at chromosome 22 in both individuals (Figure 1); these results suggested vertical germline transmission.

However, discontinuation of antiviral treatment led to a deterioration of the patient's HPS. Because no other pathogen was detected, activation of HHV-6 was suspected. To confirm this suspicion, we performed 3 assays that could detect viral activation despite the presence of integrated HHV-6 DNA. First, reverse transcription polymerase chain reaction (RT-PCR) was used to detect viral RNA in whole-blood samples. RT-PCR was performed on 2 HHV-6 genes, the late gene U60/66 and the immediate-early (IE) gene IE1, as described previously [5]. We detected viral RNA for both genes (4.6×10^2 copies/μg RNA for U60/66 and 5.2×10^3 copies/μg RNA for IE1). Second, immunostaining was used to detect IE antigens in a bone marrow sample taken at the time of HPS (Figure 2 and Supplementary Figure 2) [6]. Last, HHV-6A was isolated from the patient's PBMCs. It was cultured with cord blood cells and its presence confirmed by immunofluorescent staining with an anti–HHV-6 monoclonal antibody (Figure 3 and Supplementary Figure 3) [1].

Two hypotheses were postulated: Either the patient with ciHHV-6 was infected de novo with HHV-6, or HHV-6 was activated from the ciHHV-6 genome present in this patient. We performed a sequence analysis of the HHV-6 IE1 gene, as IE1 is variable and readily used to distinguish between HHV-6 variants [7]. DNA samples from isolated HHV-6A (described above), the patient's fingernails, his father's hair follicles, and laboratory strains U1102 and Z29 were amplified by PCR and sequenced. Because active HHV-6 is not present in the fingernails or hair follicles, we could amplify the original integrated HHV-6 strain from the genomes in these tissues. To our surprise, the sequences and subsequent phylogenetic analysis revealed that the isolated virus was identical to the original integrated HHV-6A strain present in both the patient and his father. Furthermore, this HHV-6A strain was unique in that it differed from all other HHV-6 strains analyzed (Supplementary Figure 4). These results suggested that the isolated HHV-6A strain originated from the activation of ciHHV-6A. Analysis of 3 other viral genes (gB, U94, and DR) confirmed these results [8, 9].

The resumption of antiviral drug treatment with prednisolone ameliorated the patient's HPS. When he reached age 7 months, the patient underwent HSCT. Antiviral drug treatment was continued during HSCT, and engraftment was achieved 14 days after transplant. After engraftment, thrombotic microangiopathy (TMA) and gastrointestinal bleeding developed. Simultaneously, the patient's HHV-6A DNA and RNA titers increased, and HHV-6A was reisolated. Anticoagulant therapy and a reduction in tacrolimus dosage gradually improved the patient's TMA. With immunological reconstruction, the patient's HHV-6A DNA and RNA titers were successfully reduced and ultimately, no HHV-6A was isolated from subsequent blood samples. The asymptomatic patient was discharged at 12 months.

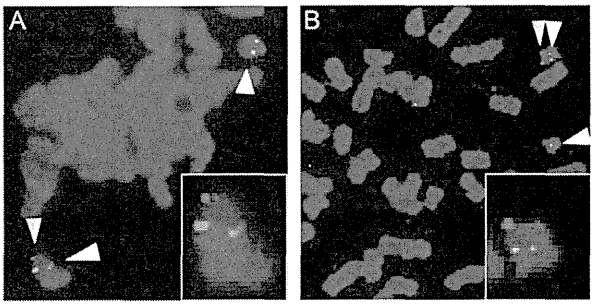

Figure 1. Integration of human herpesvirus type 6 (HHV-6) in chromosome 22 was demonstrated by fluorescence in situ hybridization analysis. Fibroblasts derived from the patient's skin (*A*) and peripheral blood mononuclear cells from the father (*B*) were cohybridized with HHV-6-specific (yellow arrow) and chromosome-22-specific probes (white arrows) [4]. HHV-6 integration in only one of the chromosome 22 alleles was shown in both materials. In sets of *A* and *B* are the enlarged images of FISH data positively cohybridized with both probes.

DISCUSSION

Since the discovery of ciHHV-6 in 1993, the question of whether ciHHV-6 can be activated from its integrated state has been perpetually debated [2]. With this case report, we provide the first molecular and virological evidence of viral activation from ciHHV-6A in the human body. This evidence comprises (1) viral RNA and antigens detected in PBMCs and bone marrow, as well as HHV-6A isolated from PBMCs; (2) HHV-6A sequences integrated into the patient's and his father's genomes, which were identical to those of the isolated virus; and (3) antiviral treatment and immunological reconstruction, which were effective in treating this activated ciHHV-6A.

In an effort to understand the biological significance of ciHHV-6, active viral replication from ciHHV-6 has recently been demonstrated in vitro under specific experimental conditions [9–11]. However, only a few studies have suggested ciHHV-6 activation in vivo despite high ciHHV-6 prevalence (approximately 1%) in the general population [12–14]. Activation of ciHHV-6 in vivo has been previously reported in mothers with ciHHV-6 who passed on the infection to infants who did not have inherited ciHHV-6 [8]. Our findings are consistent with these findings, as we clearly demonstrate the activation of HHV-6A in a patient who acquired ciHHV-6 via germline transmission.

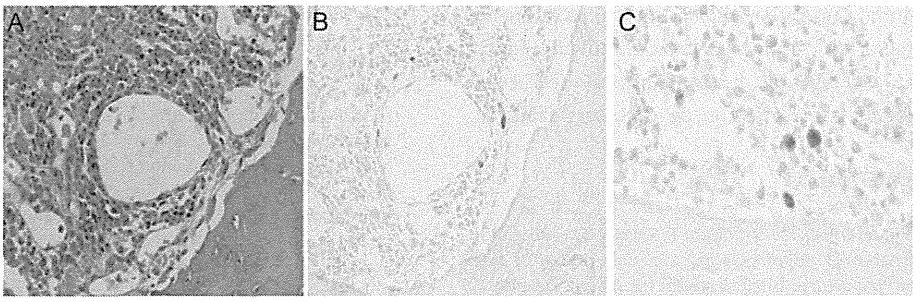

Figure 2. Histology and human herpesvirus type 6 (HHV-6) immunostaining. *A*, Hematoxylin and eosin staining of bone marrow. *B* and *C*, Immunostaining with an anti–HHV-6 antibody.

We speculate that the presence of X-SCID allowed for efficient activation of ciHHV-6A, and this phenomenon was detected with several technical strategies. Similarly, RT-PCR and virus isolation showed conversion from an HHV-6–positive status to a negative status with the patient's immunological recovery. In addition, these techniques were used to test samples taken from the patient's father. We were able to determine that he was indeed the ciHHV-6 carrier, yet he was HHV-6A negative. This suggests that X-SCID influenced the activation of ciHHV-6A. Because X-SCID prevalence is extremely low (about 0.001%), this case provides valuable insight into immunocompromised individuals and HHV-6 infection. However, the mechanism that triggered ciHHV-6A activation and replication in this patient remains to be elucidated. Further studies of patients with ciHHV-6 are required to determine what causes activation of this latent integrated virus.

The association between HHV-6 and HPS has previously been reported [15], and a link between HHV-6 and TMA has also been noted [16]. Therefore, it is possible that ciHHV-6A activation in our patient was associated with HPS and TMA. We noted that active HHV-6A infection coincided with symptom onset and the active infection was controlled with antiviral treatment. This suggests that HHV-6A is pathogenic, yet it remains to be established whether activated HHV-6A enhances underlying pathological conditions, and whether the activation of ciHHV-6A occurs in a similar fashion for all infected individuals.

Latent HHV-6 reactivation occurs in 40%–50% of recipients during HSCT, and our case report is the first to demonstrate that ciHHV-6A activation also occurs during this procedure. It is possible that the presence of X-SCID allowed for viral activation, but further studies are required to validate this hypothesis.

We have described the first case to provide molecular and virological evidence of the activation of chromosomally integrated HHV-6A in the human body. However, our report has limitations. We still do not know how virus production was triggered from a state of ciHHV-6A or how the production of the virus affected the patient's symptoms. Despite these limitations, based on this case, we hypothesize that an immunodeficient phenotype in conjunction with uncontrolled host defense systems allows the activation of ciHHV-6A. We support the recommendation that a screening program to detect ciHHV-6 in

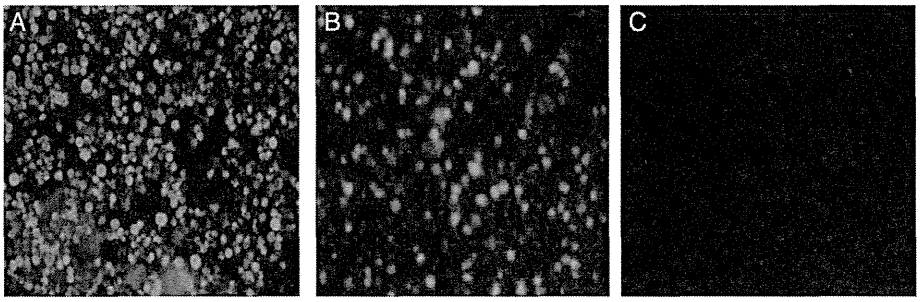

Figure 3. Immunofluorescent staining assay. *A*, Virus isolation confirmed with an anti– human herpesvirus type 6 antibody (gp116/64/54). *B*, U1102 cultured with cord blood cells (positive control). *C*, Cord blood cells alone (negative control).

transplant patients and donors be established, and recommend that ciHHV-6 patients with immunocompromised status such as primary immunodeficiency, human immunodeficiency virus infection, or organ transplantation, be monitored carefully.

Supplementary Data

Supplementary materials are available at *Clinical Infectious Diseases* online (http://cid.oxfordjournals.org). Supplementary materials consist of data provided by the author that are published to benefit the reader. The posted materials are not copyedited. The contents of all supplementary data are the sole responsibility of the authors. Questions or messages regarding errors should be addressed to the author.

Notes

Financial support. This work was supported by the Ministry of Health, Labour, and Welfare of Japan (H25 Shinko-Ippan-015 to H. Ka., H23 Nanchi-Ippan-003 and H25 Nanchitou-Menneki-Ippan-105 to T. Mo.); the Japan Society for the Promotion of Science (22590426 to N. I.); and the Ministry of Education, Culture, Sciences, and Technology in Japan (23390270 and 23390271 to T. Mo. and S. M.).

Potential conflicts of interest. All authors: No reported conflicts.

All authors have submitted the ICMJE Form for Disclosure of Potential Conflicts of Interest. Conflicts that the editors consider relevant to the content of the manuscript have been disclosed.

References

1. Yamanishi K, Shiraki K, Kondo T, et al. Identification of human herpesvirus-6 as a causal agent for exanthema subitum. Lancet **1988**; 1: 1065–7.
2. Pellett PE, Ablashi DV, Ambros PF, et al. Chromosomally integrated human herpesvirus 6: questions and answers. Rev Med Virol **2012**; 22: 144–55.
3. Sugamura K, Asao H, Kondo M, et al. The interleukin-2 receptor gamma chain: its role in the multiple cytokine receptor complexes and T cell development in XSCID. Annu Rev Immunol **1996**; 14: 179–205.
4. Isegawa Y, Mukai T, Nakano K, et al. Comparison of the complete DNA sequences of human herpesvirus 6 variants A and B. J Virol **1999**; 73: 8053–63.
5. Van den Bosch G, Locatelli G, Geerts L, et al. Development of reverse transcriptase PCR assays for detection of active human herpesvirus 6 infection. J Clin Microbiol **2001**; 39:2308–10.
6. Papanikolaou E, Kouvatsis V, Dimitriadis G, Inoue N, Arsenakis M. Identification and characterization of the gene products of open reading frame U86/87 of human herpesvirus 6. Virus Res **2002**; 89:89–101.
7. Yamamoto T, Mukai T, Kondo K, Yamanishi K. Variation of DNA sequence in immediate-early gene of human herpesvirus 6 and variant identification by PCR. J Clin Microbiol **1994**; 32:473–6.
8. Gravel A, Hall CB, Flamand L. Sequence analysis of transplacentally acquired human herpesvirus 6 DNA is consistent with transmission of a chromosomally integrated reactivated virus. J Infect Dis **2013**; 207:1585–9.
9. Arbuckle JH, Medveczky MM, Luka J, et al. The latent human herpesvirus-6A genome specifically integrates in telomeres of human chromosomes in vivo and in vitro. Proc Natl Acad Sci U S A **2010**; 107:5563–8.
10. Prusty BK, Krohne G, Rudel T. Reactivation of chromosomally integrated human herpesvirus-6 by telomeric circle formation. PLoS Genet **2013**; 9:e1004033.
11. Huang Y, Hidalgo-Bravo A, Zhang E, et al. Human telomeres that carry an integrated copy of human herpesvirus 6 are often short and unstable, facilitating release of the viral genome from the chromosome. Nucleic Acids Res **2014**; 42:315–27.
12. Kobayashi D, Kogawa K, Imai K, et al. Quantitation of human herpesvirus-6 (HHV-6) DNA in a cord blood transplant recipient with chromosomal integration of HHV-6. Transpl Infect Dis **2011**; 13:650–3.
13. Troy SB, Blackburn BG, Yeom K, Caulfield AK, Bhangoo MS, Montoya JG. Severe encephalomyelitis in an immunocompetent adult with chromosomally integrated human herpesvirus 6 and clinical response to treatment with foscarnet plus ganciclovir. Clin Infect Dis **2008**; 47: e93–6.
14. Wittekindt B, Berger A, Porto L, et al. Human herpes virus-6 DNA in cerebrospinal fluid of children undergoing therapy for acute leukaemia. Br J Haematol **2009**; 145:542–5.
15. Tanaka H, Nishimura T, Hakui M, Sugimoto H, Tanaka-Taya K, Yamanishi K. Human herpesvirus-6-associated hemophagocytic syndrome in a healthy adult. Emerg Infect Dis **2002**; 8:87–8.
16. Matsuda Y, Hara J, Miyoshi H, et al. Thrombotic microangiopathy associated with reactivation of human herpesvirus-6 following high-dose chemotherapy with autologous bone marrow transplantation in young children thrombotic microangioapathy. Bone Marrow Transplant **1999**; 24:919–23.

Journal of General Virology (2014), 95, 2576–2588 DOI 10.1099/vir.0.066225-0

Ultrasensitive detection of PrP^{Sc} in the cerebrospinal fluid and blood of macaques infected with bovine spongiform encephalopathy prion

Yuichi Murayama,[1] Kentaro Masujin,[1] Morikazu Imamura,[1] Fumiko Ono,[2] Hiroaki Shibata,[3] Minoru Tobiume,[4] Tomoaki Yamamura,[1] Noriko Shimozaki,[1] Keiji Terao,[3] Yoshio Yamakawa[5] and Tetsutaro Sata[4]

Correspondence
Yuichi Murayama
ymura@affrc.go.jp

[1]Influenza and Prion Disease Research Center, National Institute of Animal Health, Tsukuba, Ibaraki, Japan

[2]Chiba Institute of Science Faculty of Risk and Crisis Management, Choshi, Chiba, Japan

[3]Tsukuba Primate Research Center, National Institute of Biomedical Innovation, Tsukuba, Ibaraki, Japan

[4]Department of Pathology, National Institute of Infectious Diseases, Tokyo, Japan

[5]Department of Biochemistry and Cell Biology, National Institute of Infectious Diseases, Tokyo, Japan

Prion diseases are characterized by the prominent accumulation of the misfolded form of a normal cellular protein (PrP^{Sc}) in the central nervous system. The pathological features and biochemical properties of PrP^{Sc} in macaque monkeys infected with the bovine spongiform encephalopathy (BSE) prion have been found to be similar to those of human subjects with variant Creutzfeldt–Jakob disease (vCJD). Non-human primate models are thus ideally suited for performing valid diagnostic tests and determining the efficacy of potential therapeutic agents. In the current study, we developed a highly efficient method for *in vitro* amplification of cynomolgus macaque BSE PrP^{Sc}. This method involves amplifying PrP^{Sc} by protein misfolding cyclic amplification (PMCA) using mouse brain homogenate as a PrP^{C} substrate in the presence of sulfated dextran compounds. This method is capable of amplifying very small amounts of PrP^{Sc} contained in the cerebrospinal fluid (CSF) and white blood cells (WBCs), as well as in the peripheral tissues of macaques that have been intracerebrally inoculated with the BSE prion. After clinical signs of the disease appeared in three macaques, we detected PrP^{Sc} in the CSF by serial PMCA, and the CSF levels of PrP^{Sc} tended to increase with disease progression. In addition, PrP^{Sc} was detectable in WBCs at the clinical phases of the disease in two of the three macaques. Thus, our highly sensitive, novel method may be useful for furthering the understanding of the tissue distribution of PrP^{Sc} in non-human primate models of CJD.

Received 24 March 2014
Accepted 10 July 2014

INTRODUCTION

Transmissible spongiform encephalopathies (TSEs), commonly known as prion diseases, are fatal neurodegenerative disorders that affect both animals and humans (Collinge, 2001). Prion diseases are characterized by the prominent accumulation of a misfolded prion protein, PrP^{Sc}, in the central nervous system (Prusiner, 1991, 1998). PrP^{Sc}, which is rich in beta-sheet structures and resistant to digestion by proteases and various inactivating treatments (Caughey *et al.*, 1991; Pan *et al.*, 1993), is considered to be the infectious agent for TSEs and appears to self-propagate through post-translational modification of the normal prion protein PrP^{C} (Prusiner, 1998).

One type of human prion disease, Creutzfeldt–Jakob disease (CJD), can be aetiologically identified as sporadic, inherited or acquired by infection (Ironside, 1998; Belay, 1999; Glatzel *et al.*, 2002; Geissen *et al.*, 2007). In variant CJD (vCJD), which is a form of CJD caused by consumption of foods contaminated with bovine spongiform encephalopathy (BSE) prions (Will *et al.*, 1996; Hill *et al.*, 1997; Ironside, 2010), small amounts of PrP^{Sc} have been found in a broad range of peripheral tissues, including the lymph nodes, tonsils, spleen, kidneys, portions of the intestinal tract and skeletal muscle (Wadsworth *et al.*, 2001; Hilton *et al.*, 2004; Peden *et al.*, 2006; Notari *et al.*, 2010), as well as in the

Four figures and one table are available with the online version of this paper.

central nervous system. These observations have led to serious concerns that the disease could spread in humans via blood transfusions (Wroe *et al.*, 2006; Knight, 2010) and through the use of contaminated biological and surgical instruments. In order to effectively prevent the spread of this disease, it is important to be able to detect PrP^{Sc} as soon after infection as possible, and then, it is crucial to avoid PrP^{Sc} contamination in human-derived materials. As the concentration of PrP^{Sc} in the tissues or body fluids of infected subjects is predicted to be extremely low until marked clinical signs appear, development of both a sensitive method for detecting PrP^{Sc} and animal models to confirm its validity are necessary.

Several studies have used non-human primates to study the transmissibility of human prion diseases (Gajdusek *et al.*, 1966; Gibbs *et al.*, 1968), and the transmissibility of BSE has specifically been investigated using macaque monkeys (Lasmézas *et al.*, 1996, 2005; Comoy *et al.*, 2008; Ono *et al.*, 2011a, b). These studies have reported a number of advantages of using non-human primate models of prion disease. For example, the pathological feature of florid plaques in the brain tissue of BSE-infected macaques and the biochemical characteristics of the PrP^{Sc} glycoform profile in these macaques have been shown to be identical to those in human subjects with vCJD (Lasmézas *et al.*, 1996). In macaques inoculated with the BSE prion either intracerebrally or orally and in humans infected with vCJD, PrP^{Sc} has been found to be distributed in various peripheral tissues, such as the lymph nodes, spleen, tonsils and muscles. These findings strongly support the possibility that vCJD is caused by an exogenous infection of a BSE prion. Furthermore, BSE can be transmitted via intravenous inoculation (Lasmézas *et al.*, 2001), indicating that macaques can serve as model animals for suspected cases of secondary transmission (via blood transfusion) of vCJD in humans. Therefore, non-human primate models are ideally suited for assessing methods for diagnosis and treatment of prion diseases.

In scrapie-infected rodents (Brown *et al.*, 1998) and sheep (Houston *et al.*, 2008) as well as in deer with chronic wasting disease (CWD), bodily fluids such as the blood, urine, saliva and faeces have been reported to be infectious (Mathiason *et al.*, 2006; Haley *et al.*, 2009b; Mathiason *et al.*, 2010). By using the protein misfolding cyclic amplification (PMCA) technique, which amplifies PrP^{Sc} *in vitro* using normal brain homogenates as the PrP^{C} substrate, PrP^{Sc} has been detected in a variety of bodily fluids, including the blood, cerebrospinal fluid (CSF), urine, faeces, saliva and milk of prion-infected animals (Saborio *et al.*, 2001; Saá *et al.*, 2006; Murayama *et al.*, 2007, 2010; Thorne & Terry, 2008; Terry *et al.*, 2009; Maddison *et al.*, 2009, 2010; Haley *et al.*, 2009a, 2011; Tattum *et al.*, 2010; Gough *et al.*, 2012). Furthermore, several reports have described the successful detection of PrP^{Sc} in bodily fluids of humans with CJD (Orrú *et al.*, 2009; Atarashi *et al.*, 2011; Edgeworth *et al.*, 2011; Peden *et al.*, 2012; Rubenstein & Chang, 2013). For example, PrP^{Sc} in the CSF of patients with sporadic CJD (sCJD) and vCJD has been detected using the quaking-induced conversion technique (Atarashi *et al.*, 2007), which detects PrP^{Sc}-triggered formation of amyloid fibrils of recombinant prion proteins. Similarly, PrP^{Sc} has been detected in the CSF of patients with sCJD using PMCA followed by a sensitive immunoassay termed SOFIA (Rubenstein & Chang, 2013), and bead-captured ELISA has been used to detect blood PrP^{Sc} in patients with vCJD (Edgeworth *et al.*, 2011). Therefore, bodily fluids may have high utility as diagnostic materials for CJD. However, the quantitative changes of PrP^{Sc} in bodily fluids of non-human primate models of CJD has not yet been determined due to a lack of sensitive methods for assessing very small amounts of prions in these animal models.

In the present study, we have developed a highly efficient PMCA method suitable for cynomolgus macaque BSE PrP^{Sc} amplification. This method, which involves amplifying PrP^{Sc} using xenogeneic (mouse) PrP^{C} substrate in the presence of sulfated dextran compounds, is capable of amplifying a very small amount of PrP^{Sc} from the CSF, blood, and peripheral tissue of BSE-infected macaques. We further investigated CSF and blood PrP^{Sc} levels during the period from the latent to terminal stages of the disease and compared PrP^{Sc} dynamics in macaques.

RESULTS

Amplification of cynomolgus macaque BSE PrP^{Sc} by PMCA

We first examined the amplification efficiency of PMCA, using the brain homogenate of BSE-infected cynomolgus macaque no. 7 as the PrP^{Sc} seed. Before amplification, distinct signals of protease-resistant PrP (PrP^{res}) were detected in brain homogenates diluted up to 10^{-2} by Western blot analysis (Fig. 1a). In the absence of potassium dextran sulfate (DSP), brain homogenates derived from the squirrel monkey and cynomolgus macaque were not suitable for amplification of cynomolgus PrP^{Sc} (Fig. 1b, upper panel). Similarly, no significant amplification was observed using cow, TgBoPrP and $PrP^{0/0}$ mice (Fig. 1b, middle panel), or hamster brain homogenates (Fig. 1b, lower panel) as PrP^{C} substrates. On the other hand, amplification of PrP^{Sc} was achieved in samples diluted to 10^{-3} and 10^{-4} when the WT mouse brain homogenate was used as the PrP^{C} substrate (Fig. 1b, lower panel). Furthermore, amplification efficiency of mouse PrP^{Sc} for PMCA was significantly improved in the presence of DSP, and PrP^{res} signals were detected in samples diluted to 10^{-5} after one round of amplification. On the other hand, DSP was less effective in increasing signal intensity of PrP^{res} after amplifications derived using squirrel monkey, cynomolgus macaque, cow, TgBoPrP mouse and hamster brain homogenates. The detection sensitivity for cynomolgus PrP^{Sc} for these PCMAs was lower than for PMCAs conducted using WT mouse brain homogenate. Higher background signal in the no-seed samples was observed after amplification was conducted using macaque brain homogenate in the presence of DSP.

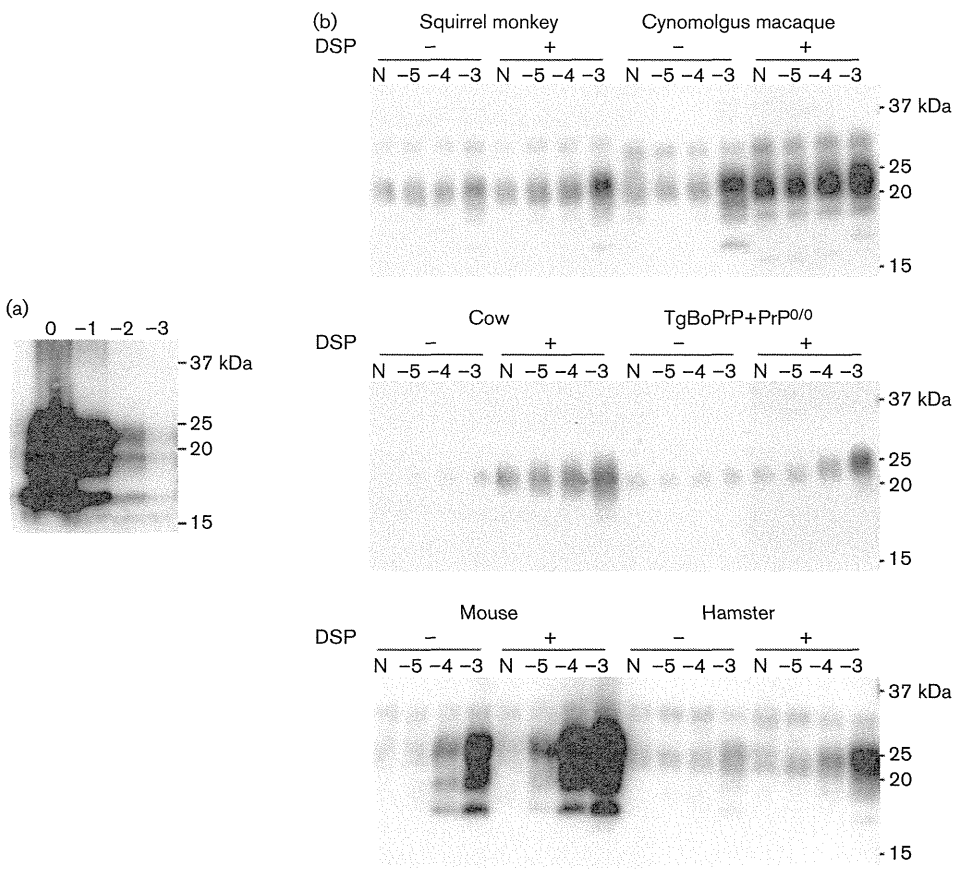

Fig. 1. Amplification of macaque PrP^{Sc} using normal brain homogenates derived from several animal species as PrP^{C} substrates. (a) Ten per cent brain homogenate of BSE-affected cynomolgus macaque was diluted to 10^{-1} (−1) to 10^{-3} (−3) in a normal macaque brain homogenate, an undiluted sample (0) was also included. The diluted samples were analysed by Western blot after digestion with proteinase K (PK). (b) PrP^{Sc} seed (10 % brain homogenate of BSE-affected cynomolgus macaque) was diluted to 10^{-3} (−3) to 10^{-5} (−5) in normal brain homogenates obtained from the squirrel monkey, cynomolgus macaque, cow, mixture of TgBoPrP and $PrP^{0/0}$ (TgBoPrP+$PrP^{0/0}$) mice, mouse and hamster. The diluted samples were amplified in the presence (+) or absence (−) of 1 % (w/v) DSP. After amplification, the samples were digested with PK and analysed by Western blot. 'N' denotes unseeded control samples in which normal brain homogenate that did not receive a PrP^{Sc} seed were processed and analysed in the same manner as PrP^{Sc}-seeded samples. The molecular masses of marker proteins are indicated (kDa).

Detection sensitivity of cynomolgus macaque BSE PrP^{Sc}

PMCA using WT mouse brain homogenate containing DSP as the PrP^{C} substrate was used for amplification of cynomolgus macaque PrP^{Sc}. On the basis of our preliminary experiments, the optimal concentration of DSP was estimated to be 1 % (w/v); therefore, we used 1 % (w/v) DSP for subsequent experiments. We determined the detection limit of the interspecies PMCA technique and confirmed that PrP^{Sc} present in a 10^{-5} dilution of infected brain homogenate could be detected after one round of amplification, and both 10^{-6} and 10^{-7} dilutions were positive for PrP^{Sc} after two rounds of amplification (Fig. 2a). After three rounds of amplification, PrP^{res} signals were detected in the samples diluted to 10^{-8} and 10^{-9}. A PrP^{res} signal was detected in the 10^{-10} dilution samples after four rounds of amplification, but almost no signal was detected in the more extreme dilutions, even after seven rounds of amplification. Thus, compared with no amplification, amplification improved the PrP^{Sc} detection sensitivity by a factor of 10^{8}. No typical PrP^{res} signal was detected in samples that contained normal brain homogenate diluted 1 : 10 with mouse PrP^{C} substrate (Fig. 2b). In addition, the generation of spontaneous PrP^{res}, as has been reported for amplification in the presence of polyanions (Deleault *et al.*, 2007; Wang *et al.*, 2010), was not observed in 16 samples that contained only mouse PrP^{C} substrate following seven rounds of amplification (Fig. 2c).

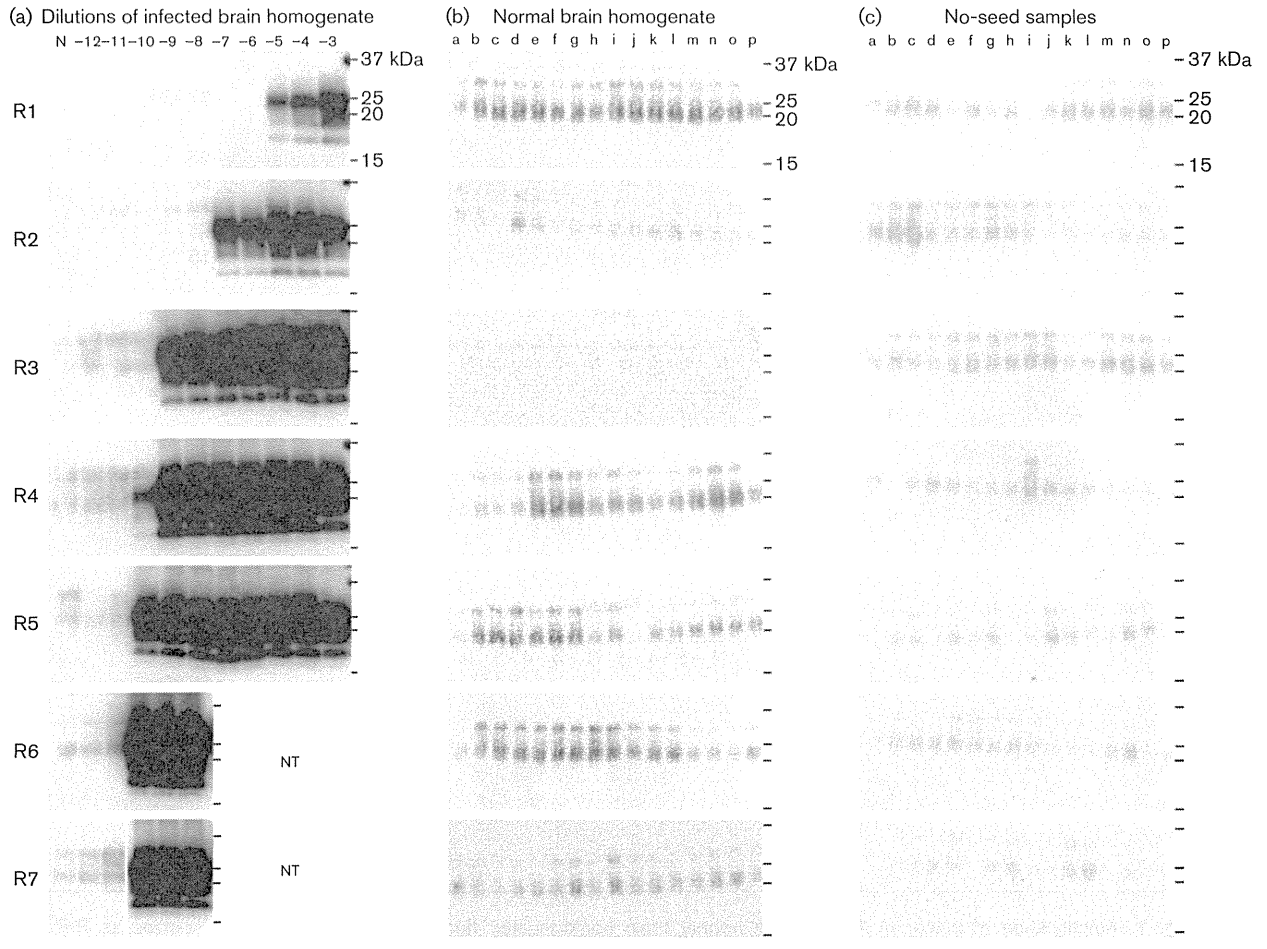

Fig. 2. Detection sensitivity for cynomolgus macaque PrP^{Sc}. (a) PrP^{Sc} seed was diluted to 10^{-3} (−3) to 10^{-12} (−12) with PrP^{C} substrate (10 % normal mouse brain homogenate), and the samples were serially amplified in the presence of 1 % (w/v) DSP. The amplified samples were analysed after each round of amplification (R1–R7) by Western blot after proteinase K (PK) digestion. (b) Normal brain homogenate was diluted to 10^{-1} with the PrP^{C} substrate (lanes a–p), and the samples were serially amplified in the presence of 1 % (w/v) DSP. After amplification, a band with a molecular mass similar to that for PrP^{Sc} was occasionally observed, which likely corresponds to a residue of the normal isoform of prion protein resulting from incomplete PK digestion. (c) No spontaneous generation of PrP^{Sc} was observed in no-seed samples. Lanes a–p contained only PrP^{C} substrate and were amplified in the presence of 1 % (w/v) DSP. Exclusive pipettes, a vortex mixer, and a centrifuge were used for handling unseeded samples. The molecular masses of marker proteins are indicated (kDa). NT, Not tested.

PrP^{Sc} distribution in the peripheral tissues of BSE-affected macaques

We examined PrP^{Sc} distribution in macaques that were intracerebrally administered a brain homogenate prepared from a BSE-infected cow. In BSE-infected macaques, PrP^{Sc} was detected by conventional Western blot analysis in several peripheral nervous tissues and lymph nodes (Table S1, available in the online Supplementary Material). By using serial PMCA, PrP^{Sc} was detected in all examined tissues, including: the peripheral nerves, lymph nodes, spleens, tonsils and adrenal glands (Fig. 3). Most samples were found to be positive for PrP^{Sc} after no more than two rounds of amplification. On the other hand, PrP^{Sc} was detected after three rounds of amplification in four and two of the quadruplicate samples of the tonsil of macaque no. 10 (Fig. 3b) and spleen of macaque no. 11 (Fig. 3c), respectively. No typical PrP^{res} signal was detected in the peripheral nerves, lymph nodes, ileum and glands of an uninfected control macaque (Fig. S1).

PrP^{Sc} levels in the CSF

The amplification results for the CSF samples collected from the three macaques are illustrated in Fig. 4. No typical PrP^{res} signal was observed in samples that contained only

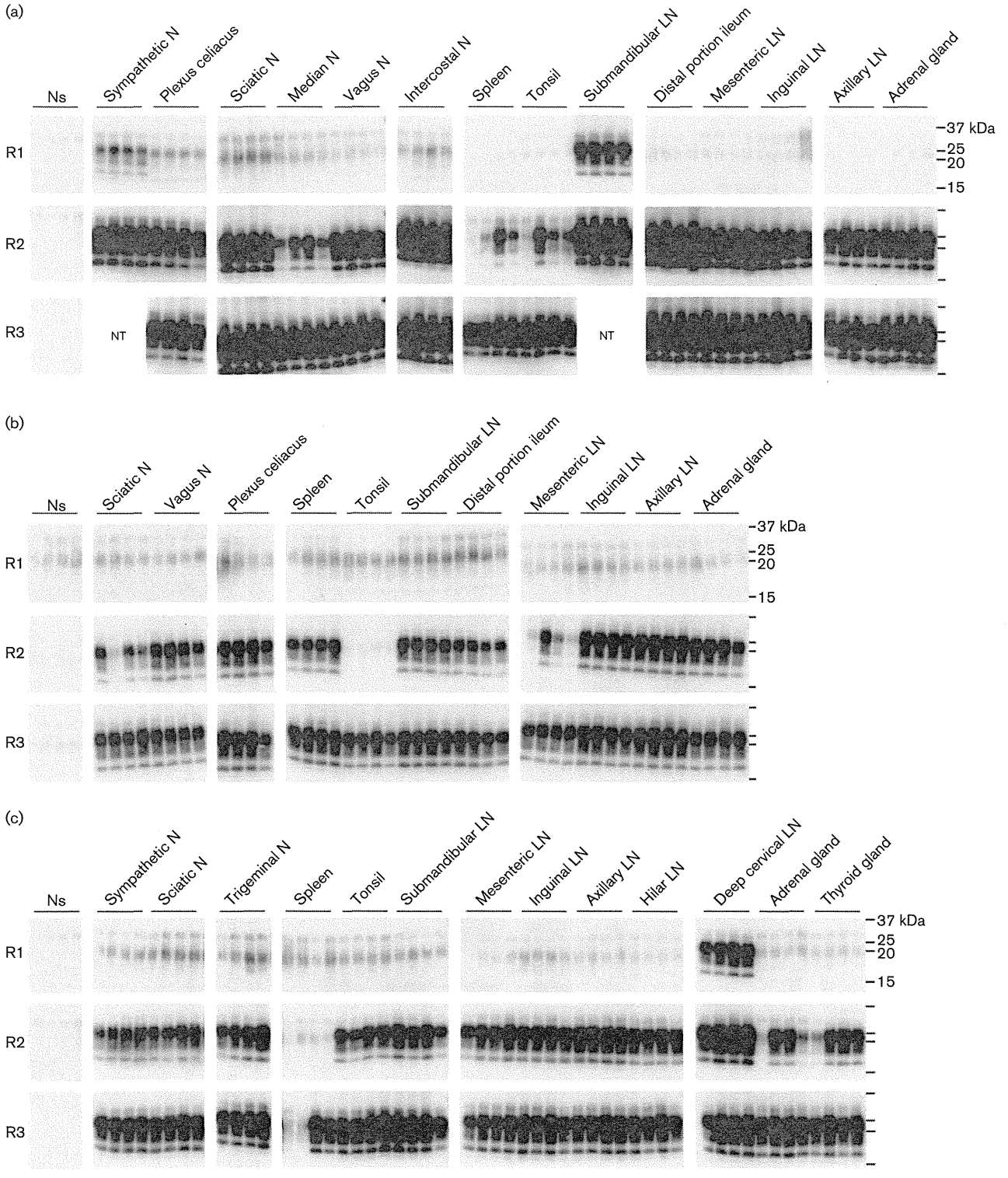

Fig. 3. Tissue distribution of PrP^{Sc} in macaques intracerebrally inoculated with BSE. Tissue distribution of PrP^{Sc} in the terminal disease stage in macaque no. 7 (a), no. 10 (b) and no. 11 (c). Quadruplicate samples of each tissue were serially amplified, and the samples were analysed by Western blot following digestion with proteinase K after each round of amplification (R1–R3). The molecular masses of marker proteins are indicated (kDa). N, Nerve; LN, lymph node; Ns, no-seed samples; NT, not tested.

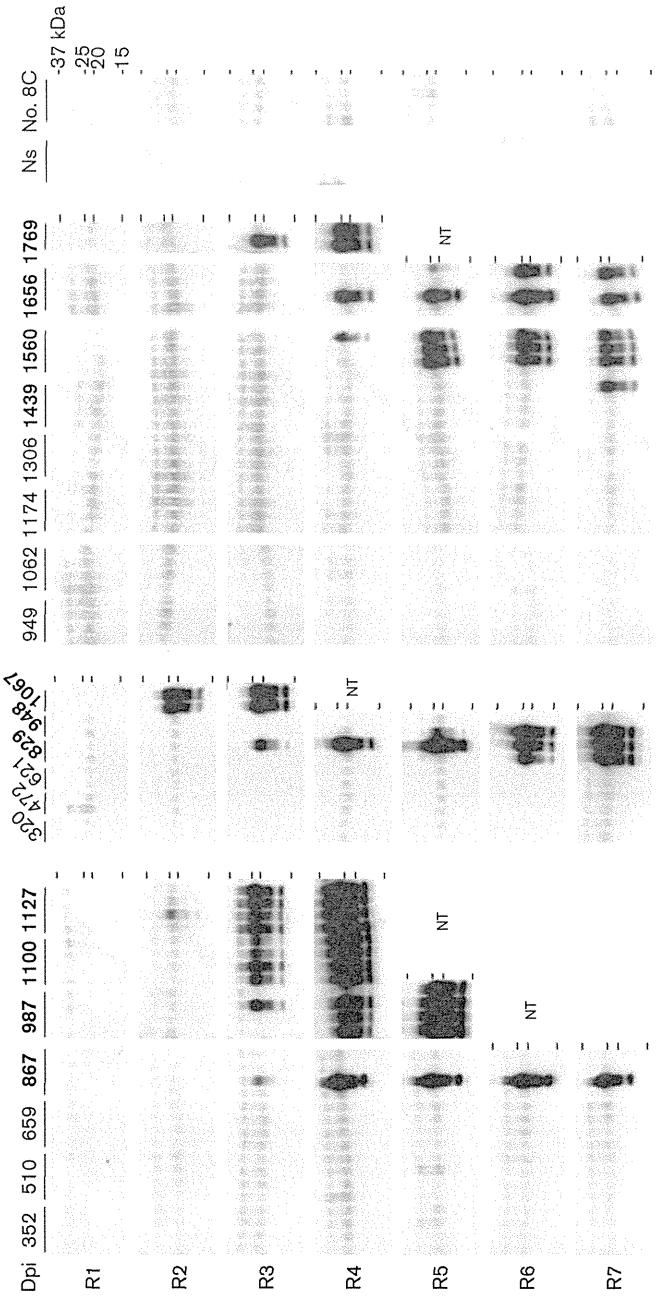

Fig. 4. The appearance of PrP^{Sc} in the cerebrospinal fluid (CSF) of BSE-infected macaques. CSF was collected at several points after intracerebral inoculation. Quadruplicate or duplicate CSF samples from BSE-infected macaque no. 7, no. 10, and no. 11 were analysed by Western blot following digestion with proteinase K after each round of amplification (R1–R7). PrP^{Sc} was also evaluated in CSF samples from an uninfected control macaque (no. 8C). Dpi, Days post-inoculation. Dpi written in boldface represents clinical stages of the disease. The molecular masses of marker proteins are indicated (kDa). Ns, No-seed samples; NT, not tested.

mouse PrP^C substrate (lanes Ns), or samples that contained normal macaque CSF diluted 1 : 10 with mouse PrP^C substrate (Fig. 4, no. 8C and Fig. S2). PrP^{res} signal was not detected in the samples collected 515–208 (macaque no. 7), 509–208 (macaque no. 10) and 490–133 days (macaque no. 11) before disease onset. The existence of PrP^{Sc} in the CSF samples was confirmed after the onset of clinical signs. For example, macaque no. 7 presented with early neurological clinical signs of the disease such as slight tremor, startle response and festinating gait. PrP^{res} signal was detected after four rounds of amplification in one of the quadruplicate samples collected at this time [867 days post-inoculation (p.i.)], but no other sample was positive for PrP^{Sc} even after seven rounds of amplification. Consistent with disease progression, macaque no. 7 presented with ataxia, paralysis of the extremities and rigidity; PrP^{Sc} was detected in all of the quadruplicate samples obtained at 987 days p.i. after five rounds of amplification. The macaque finally developed severe dysstasia, and after three rounds of amplification, PrP^{Sc} was detected in all of the quadruplicate samples obtained at 1100 days p.i. and at the dissection (1127 days p.i.). These observations suggested that the level of PrP^{Sc} tended to increase in the CSF as the disease progressed. Although a similar tendency was observed in other macaques, there were differences in the levels of PrP^{Sc} in the CSF. For example, duplicate CSF samples collected upon dissection (1067 days p.i.) became positive for PrP^{Sc} after two rounds of amplification in macaque no. 10, which showed the shortest latent period of 828 days. On the other hand, the disease developed after a relatively longer latent period of over 1400 days in macaque no. 11, and PrP^{res} signals were detected after four rounds of amplification in both samples collected upon dissection (1769 days p.i.).

PrP^{Sc} levels in the blood

The results of the amplification of white blood cell (WBC) samples collected at several time points after intracerebral administration are illustrated in Fig. 5. No typical PrP^{res} signal was observed in samples that contained only mouse PrP^C substrate (Fig. 5, lanes Ns), or samples that contained normal macaque WBCs (10^4 cells) (Fig. 5, no. 8C and Fig. S2). Furthermore, we confirmed that the WBC matrix had no inhibitory effect on the amplification of PrP^{Sc} by serial PMCA (Fig. S3). In macaque no. 7, one of the quadruplicate samples collected upon dissection (1127 days p.i.) became positive for PrP^{Sc} after five rounds of amplification. Similarly, PrP^{res} signal was detected in one or both of the duplicate samples of macaque no. 11 collected at 1656 days p.i., and at dissection (1769 days p.i.). However, PrP^{Sc} was not detected in the blood of these macaques between the latent and the initial stage of disease onset. In macaque no. 10, PrP^{res} signal was not detected in the WBCs obtained during the experimental period (320–1067 days p.i.) even after seven rounds of amplification. With regard to plasma samples, no PrP^{Sc} was detected in any of the samples collected during the experimental period (data not shown).

Infectivity of the PMCA product

The PMCA product obtained after ten rounds of amplification was diluted 10-fold and inoculated intracerebrally into tga20 mice. The tga20 mice inoculated with the PMCA products derived from the brain or WBC PrP^{Sc} seeds died after an average period of 305 or 310 days, respectively (Table 1). PrP^{Sc} accumulation in the brains of mice was confirmed by Western blot analysis (data not shown). There was no significant difference between the survival periods of these PMCA product-inoculated mice (*t*-test, $P>0.05$). Control mice administered with the product containing only PrP^C substrate survived more than 478 days. These results indicated that both brain- and WBC-derived PrP^{Sc} had seeding activities following the PMCA reactions, and the amplified PrP^{Sc} maintained their infectious ability during *in vitro* xenogeneic amplification.

DISCUSSION

In the current study, we developed an ultra-efficient PMCA technique for amplifying PrP^{Sc} derived from BSE-infected cynomolgus macaques by using mouse brain homogenates with DSP as a PrP^C substrate and a polyanion additive, respectively. We first proved the existence of PrP^{Sc} in the CSF and blood of BSE-infected macaques by PMCA, and showed that cynomolgus macaque BSE PrP^{Sc}, and non-macaque PrP^C, effectively converted mouse PrP^C to a proteinase K (PK)-resistant form. It is well known that PMCA of several xenogeneic combinations of PrP^{Sc} seed and PrP^C substrate can overcome the species barrier (Kurt *et al.*, 2007, 2011; Green *et al.*, 2008; Castilla *et al.*, 2008; Yoshioka *et al.*, 2011; Murayama *et al.*, 2012; Nemecek *et al.*, 2013), despite the divergent amino acid sequence of prion proteins. Since the BSE prion was transmissive to ICR (WT) mice (Masujin *et al.*, 2008), the cynomolgus macaque PrP^{Sc} generated by the cross-species transmission of BSE prion may retain the original characteristics of BSE PrP^{Sc}, including structural compatibility with mouse PrP^C and DSP dependency in PMCA reactions.

PrP^{Sc} is detectable in the tonsil, spleen and lymph nodes in vCJD (Wadsworth *et al.*, 2001) and sCJD patients (Rubenstein & Chang, 2013). In an earlier study, PrP^{Sc} was found in the lymphoid tissues, including: the lymph nodes, spleens and tonsils of macaques intracerebrally inoculated with BSE PrP^{Sc} (Lasmézas *et al.*, 1996), as observed in vCJD-inoculated macaques (Lasmézas *et al.*, 2001). Therefore, once PrP^{Sc} accumulates in the brain, it may spread centrifugally from the brain to the peripheral tissues through the autonomic nervous system. However, in our previous study, we failed to detect PrP^{Sc} in such lymphoid tissues of the BSE-inoculated macaques by conventional Western blotting, except in the submandibular lymph nodes, deep cervical lymph nodes and inguinal lymph nodes (Ono *et al.*, 2011a; Table S1). In the current study, PMCA analysis revealed that PrP^{Sc} was distributed in all lymphoid tissues examined in the BSE-infected macaques.

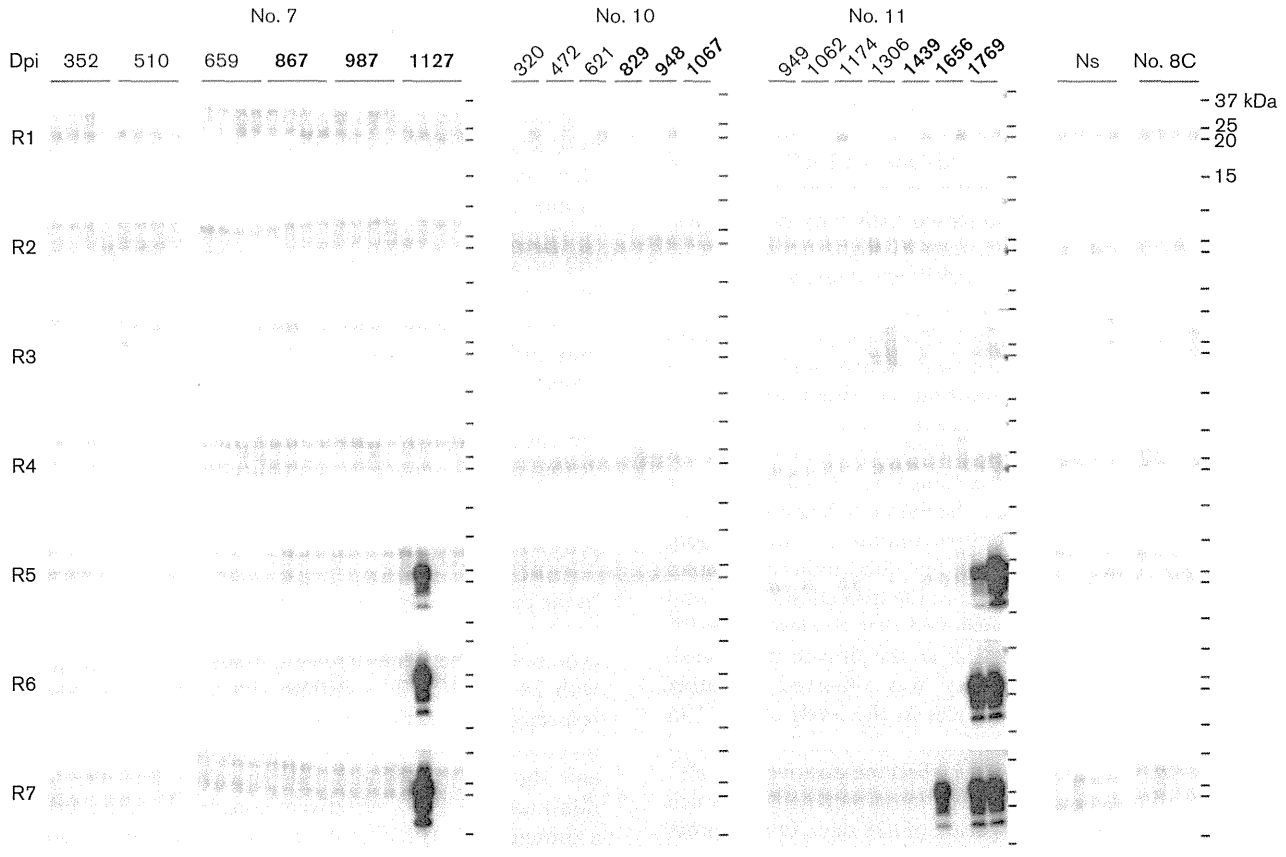

Fig. 5. Appearance of PrP^{Sc} in the WBCs of BSE-infected macaques. WBCs were collected at several points after intracerebral inoculation. Quadruplicate or duplicate WBC samples from BSE-infected macaque no. 7, no. 10 and no. 11 were analysed by Western blot following digestion with proteinase K after each round of amplification (R1–R7). PrP^{Sc} was also evaluated in WBCs from an uninfected control macaque (no. 8C). Dpi, Days post-inoculation. Dpi written in boldface represents the clinical stages of the disease. The molecular masses of marker proteins are indicated (kDa). Ns, No-seed samples.

PrP^{Sc} levels in most of the lymphoid tissues were extremely low, because PrP^{Sc} could only be detected after two or three rounds of amplification. Therefore, significant PrP^{Sc} accumulation in the peripheral non-neuronal tissues might not have occurred in these macaques, and PrP^{Sc} levels in most lymphoid tissues might have been below the detection limit of the conventional Western blot technique used herein, even at the terminal stage of the disease.

Table 1. Mean incubation time following intracerebral inoculation in tga20 transgenic mice

Inoculum (R10 PMCA product)	Transmission rate (total death/total number)	Mean survival time ± SD (days)
Brain seed*	100 % (6/6)	305 ± 10
WBCs seed†	100 % (6/6)	310 ± 23
No seed	0 % (0/4)	>478
10 % Brain homogenate from a BSE-infected cow‡	100 % (20/20)	495 ± 43

R10, Tenth round.

*The final dilution of the infected brain homogenate (macaque no. 7) in the R10 product was 6.4×10^{-11}.

†The PMCA product from the tenth round of amplification of PrP^{Sc}-positive WBCs (macaque no. 7).

‡Classical BSE (c-BSE) prion was inoculated in tga20 mice for comparison of infectivity.

The origin of PrP^{Sc} in WBCs may be the spleen and other lymphoid organs, as suggested previously (Saá *et al.*, 2006). As in humans, PrP^{C} is constitutively expressed in the WBCs of cynomolgus macaques (Holada *et al.*, 2007); therefore, WBCs of cynomolgus macaques can be deemed carriers or reservoirs of PrP^{Sc}. Our finding supports the idea that prion diseases may be transmitted via infected blood in primates, as has been previously seen in scrapie-infected sheep (Houston *et al.*, 2008) and CWD-infected deer (Mathiason *et al.*, 2006). An illustration for the appearance of PrP^{Sc} in the CSF and WBCs of intracerebrally infected macaques is shown in Fig. 6. PrP^{Sc} was found in the WBCs at clinical stages of the disease in macaques no. 7 and no. 11, but PrP^{Sc} was not detected in the WBCs of macaque no. 10 throughout the experimental period. Survival time of the BSE-infected macaques ranged from 1067 days to 1769 days. During the period from the onset of clinical signs to the terminal stage of the disease, PrP^{Sc} was detected in the CSF in all three BSE-infected macaques. The highest level of PrP^{Sc} in the CSF collected upon dissection was observed in macaque no. 10.

A previous study showed that elevated levels of 14-3-3 proteins, which are widely distributed in eukaryotes and play an important role in various signal transduction systems involved in cell proliferation and division, were observed in the CSF of a simian vCJD model (Yutzy *et al.*, 2007). The increase of PrP^{Sc} in the CSF probably reflects the leakage of PrP^{Sc} from neuronal cells after cell destruction caused by PrP^{Sc} infection. We examined 14-3-3 γ levels in the CSF of the BSE-infected macaques (Fig. S4), and found that the signal intensity of the 14-3-3 γ protein became notable after disease onset (no. 7 and no. 10), or in the latter stages of the disease (no. 11). It is worth noting that the highest levels of the 14-3-3 γ protein were observed in the CSF of macaque no. 10 collected at dissection. Therefore, the disease might have progressed most rapidly after a shorter latent period (829 days) in macaque no. 10 than in macaques no. 7 (867 days) and no. 11 (1439 days). Faster accumulation of PrP^{Sc} in the brain may cause acute brain damage and result in death before a significant number of infected WBCs begin circulating in the peripheral blood. Macaques no. 7 and 10 both belonged to a breeding colony introduced from the Philippines, and no. 11 was derived from a Malaysian lineage. Thus, the different degrees of disease progression might be related to genetic factors affecting susceptibility or resistance to prion infection.

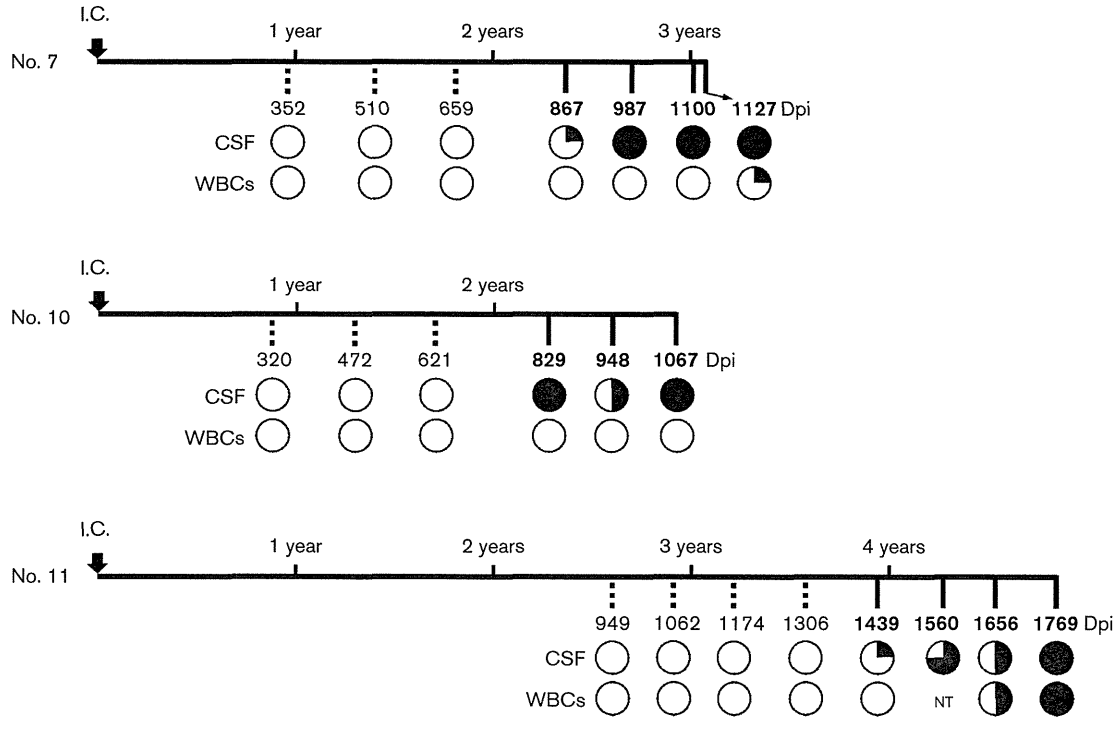

Fig. 6. Schematic illustration for the appearance of PrP^{Sc} in the CSF and WBCs of three BSE-infected macaques. After intracerebral inoculation (I. C.), the presence of PrP^{Sc} in CSF and WBCs was examined by serial PMCA during the asymptomatic (dotted line) and clinical stages (solid lines). Dpi, Days post-inoculation. Dpi written in boldface represents the clinical stages of the disease. Positive ratio of duplicate or quadruplicate samples was shown as open circle (0 %), closed quadrant (25 %), closed semicircle (50 %), closed three quadrants (75 %) and closed circle (100 %). NT, Not tested.

More detailed studies are needed to clarify the above possibility.

In conclusion, we have developed a highly sensitive method that enables a detailed and precise examination of the distribution of PrP^{Sc} throughout the bodies of BSE-infected macaques. We are now conducting experiments analysing oral transmission of the BSE prion and transmission through blood transfusions from BSE-infected macaques. Using our method, PrP^{Sc} could notably be detected in bodily fluids obtained during the latent period of the disease in both primate models. Thus, the method developed in this study may be useful in furthering the understanding of tissue distribution of PrP^{Sc} in non-human primate models of CJD.

METHODS

BSE-infected macaques. This study on non-human primates was conducted according to the rules for animal care and management of the Tsukuba Primate Research Center (Honjo, 1985) and the guiding principles for animal experiments using non-human primates formulated by the Primate Society of Japan (Primate Society of Japan, 1986). The cynomolgus macaques (*Macaca fascicularis*) examined in this study originated from the Philippines (no. 7 and 10) or Malaysia (no. 11), and were bred at Tsukuba Primate Research Center of the National Institute of Biomedical Innovation. Transmission experiments were approved by the Animal Welfare and Animal Care and Use Committee (approval ID: DS18-069R1) and Animal Ethics Biosafety Committee (approval ID: BSL3-R-06.01) of the National Institute of Biomedical Innovation. The brain homogenate (200 µl of a 10 % brain homogenate) derived from a classical BSE (c-BSE)-infected 83-month-old Holstein (Iwata *et al.*, 2006) was intracerebrally administered to three male macaques (no. 7, 10 and 11) that were 24–29 months in age (Ono *et al.*, 2011a). The animals were housed in biosafety level three animal rooms, and their clinical status was monitored daily. After 35–59 months, the animals were euthanized by anaesthesia overdose following evidence of progressive neurological dysfunction, after which the animals were dissected. A healthy macaque (no. 8 or 28) was used as an uninfected control in the PMCA assay of tissues and bodily fluids. All macaques examined in this study were homozygous for methionine at codon 129 (MM) and homozygous for glutamic acid at codon 219 (EE).

Sample preparation. Peripheral nervous and lymphoid tissues were collected upon dissection and stored in small aliquots at −80 °C. Samples from each tissue were homogenized at 10 % (w/v) in PBS. WBCs, plasma and CSF were also collected at several time points after inoculation. The blood samples (1.5 ml) were centrifuged at 1500 *g* for 15 min and the plasma and buffy coat fractions were recovered. Erythrocytes contaminated in the buffy coat fraction were haemolysed in distilled water, and the samples were stored at −80 °C until analysis.

Preparation of PrP^{C} substrates. To avoid contamination, normal brain homogenates were prepared in a laboratory in which infected materials had never been handled. Brains of a healthy cynomolgus macaque, squirrel monkey (*Saimiri sciureus*), cow, PrP^{C}-overexpressing transgenic [Tg(BoPrP) 4092HOZ/$Prnp^{0/0}$, TgBoPrP] mouse (Scott *et al.*, 1997), PrP-knockout ($PrP^{0/0}$) mouse, WT mouse (ICR), and Syrian hamster were homogenized at a 20 % (w/v) concentration in PBS containing a complete protease inhibitor cocktail (Roche Diagnostics). The brain homogenates were stored at −80 °C until further use. For analysis, the homogenates were mixed with an equal volume of the elution buffer (PBS containing 2 % Triton X-100, 8 mM EDTA) and incubated at 4 °C for 1 h with continuous agitation. After centrifugation at 4500 *g* for 5 min, the supernatant was used as the PrP^{C} substrate. When using brain homogenates of TgBoPrP mice, the supernatants were mixed in a 5 : 1 proportion of $PrP^{0/0}$:TgBoPrP, and this mixture was used as the PrP^{C} substrate.

PMCA. For the amplification of brain PrP^{Sc}, the BSE-infected brain homogenate of macaque no. 7 was diluted from 10^{-3} to 10^{-5} with normal brain homogenates from several animal species in an electron beam-irradiated polystyrene tube (total volume, 100 µl). Amplification was performed in the presence or absence of 1 % (w/v) DSP, which has been shown to markedly improve *in vitro* amplification efficiency of bovine BSE PrP^{Sc} (Murayama *et al.*, 2010). Amplification was carried out with a fully automatic cross-ultrasonic protein activating apparatus (Elestein 070-CPR; Elekon Science Corporation), which had the capacity to generate high ultrasonic power (700 W). PMCA was performed by 40 cycles of sonication in which a 3 s pulse oscillation was repeated five times at 1 s intervals, followed by incubation at 37 °C for 1 h with agitation.

To examine the sensitivity of interspecies PMCA using the mouse PrP^{C} substrate for the detection of macaque BSE PrP^{Sc}, the 10 % infected brain homogenate was serially diluted from 10^{-3} to 10^{-12} with mouse PrP^{C} substrate containing 1 % (w/v) DSP (total volume, 80 µl) in an electron beam-irradiated eight-strip polystyrene tube specially designed for PrP^{Sc} propagation (Murayama *et al.*, 2010). To obtain maximum amplification efficiency and reduce non-specific background signal in Western blot analysis, a series of amplification steps were programmed as follows: PMCA was performed with 40 cycles of sonication in which a 15 s oscillation and subsequent incubations at 31 °C for 1 h were repeated 10 times; a 15 s oscillation and subsequent incubations at 33 °C for 1 h were repeated 10 times; an intermittent oscillation (3 s pulse oscillation was repeated five times at 1 s intervals) and subsequent incubations at 35 °C for 1 h were repeated 10 times; and finally intermittent oscillations (3 s pulse oscillation was repeated five times at 1 s intervals) and subsequent incubation at 37 °C for 1 h were repeated 10 times. The amplified product obtained after the first round of amplification was diluted 1 : 5 with the PrP^{C} substrate, and a second round of amplification was performed. This process was repeated for a maximum of six times.

For amplifying PrP^{Sc} in various tissues from BSE-inoculated macaques, the mouse PrP^{C} substrate containing 1 % (w/v) DSP was mixed with a 1/10 volume of homogenized samples or bodily fluids (total volume 80 µl) in eight-strip polystyrene tubes. The WBC pellet (approx. 10^{4} cells) was dissolved in 8 µl of the elution buffer and used as a seed. Serial PMCA was then performed using the four-step amplification programme as described above.

Western blotting. After each round of amplification, samples of 10 µl were mixed with 10 µl of PK solution (100 µg PK ml^{-1}) and incubated at 37 °C for 1 h. The digested materials were mixed with 20 µl of 2× SDS sample buffer and incubated at 100 °C for 5 min. The samples were separated by SDS-PAGE and transferred onto a PVDF membrane (Millipore). After blocking, the membrane was incubated for 1 h with HRP-conjugated T2 mAb (Hayashi *et al.*, 2004; Shimizu *et al.*, 2010) at a 1 : 10 000 dilution. The T2 antibody, which recognizes a discontinuous epitope in amino acid residues 132–156 in the mouse PrP sequence, also reacts with hamster and monkey PrP. After washing, the blotted membrane was developed with Immobilon Western Chemiluminescent HRP Substrate (Millipore), according to the manufacturer's instructions. Chemiluminescence signals were analysed with the Light Capture system (ATTO).

Bioassay. A 10 % brain homogenate from BSE–infected macaque (no. 7) was diluted to 10^{-4} with WT mouse PrP^{C} substrate containing 1 % (w/v) DSP and amplified. The 1 : 5 dilution of the PMCA product